

A MeerKAT 1.28 GHz Atlas of Southern Sources in the *IRAS* Revised Bright Galaxy Sample

J. J. CONDON,¹ W. D. COTTON,¹ T. JARRETT,² L. MARCHETTI,^{2,3} A. M. MATTHEWS,^{4,1} T. MAUCH,⁵ AND M. E. MOLOKO²

¹National Radio Astronomy Observatory, 520 Edgemont Road, Charlottesville, VA 22903, USA

²Astronomy Department, University of Cape Town, Private Bag X3, Rondebosch 7701, South Africa

³INAF - Istituto di Radioastronomia, via Gobetti 101, 40129 Bologna, Italy

⁴Department of Astronomy, University of Virginia, Charlottesville, VA 22904, USA

⁵South African Radio Astronomy Observatory (SARAO), 2 Fir Street, Black River Park, Observatory, 7925, South Africa

ABSTRACT

The *IRAS* Revised Bright Galaxy Sample (RBGS) comprises galaxies and unresolved mergers stronger than $S = 5.24 \text{ Jy}$ at $\lambda = 60 \mu\text{m}$ with galactic latitudes $|b| > 5^\circ$. Nearly all are dusty star-forming galaxies whose radio continuum and far-infrared luminosities are proportional to their current rates of star formation. We used the MeerKAT array of 64 dishes to make $5 \times 3 \text{ min}$ snapshot observations at $\nu = 1.28 \text{ GHz}$ covering all 298 southern ($\text{J}2000 \delta < 0^\circ$) RBGS sources identified with external galaxies. The resulting images have $\theta \approx 7''.5$ FWHM resolution and rms fluctuations $\sigma \approx 20 \mu\text{Jy beam}^{-1} \approx 0.26 \text{ K}$ low enough to reveal even faint disk emission. The rms position uncertainties are $\sigma_\alpha \approx \sigma_\delta \approx 1''$ relative to accurate near-infrared positions, and the image dynamic ranges are DR $\gtrsim 10^4 : 1$. Cropped MeerKAT images of all 298 southern RBGS sources are available in FITS format from <https://doi.org/10.48479/dnt7-6q05>.

1. INTRODUCTION

The *IRAS* (Neugebauer et al. 1984) Revised Bright Galaxy Sample (RBGS, Sanders et al. 2003) comprises all 629 *IRAS* sources (individual galaxies or unresolved mergers) with $S(60 \mu\text{m}) \geq 5.24 \text{ Jy}$ in the extragalactic sky defined by Galactic latitude $|b| > 5^\circ$. It is the far-infrared (FIR) counterpart of the Revised Third Cambridge catalog of radio sources with $S \geq 10 \text{ Jy}$ at 178 MHz (3CR, Laing et al. 1983). These FIR and radio flux-limited samples of strong sources differ in that most of the $\lambda = 60 \mu\text{m}$ emission is from dust heated by short-lived ($\tau \lesssim 100 \text{ Myr}$) stars in nearby (median redshift $\langle z \rangle = 0.01$) star-forming galaxies (SFGs), while most of the radio sources are powered by active galactic nuclei (AGNs) in distant ($\langle z \rangle \sim 1$) radio galaxies and quasars. However, the very tight FIR/radio correlation of nearby SFGs (Helou et al. 1985) makes radio continuum emission an excellent complementary tracer of recent star formation, and the RBGS selects the brightest SFG needles in the haystack of all radio sources.

Corresponding author: James J. Condon
 jcondon@nrao.edu

The radio continuum emission from SFGs is a combination of synchrotron radiation from electrons accelerated in the supernova remnants of massive ($M > 8M_\odot$) very short-lived ($\tau < 30 \text{ Myr}$) stars and free-free emission from H II regions ionized by the most massive of those stars (Condon 1992). At decimeter wavelengths, the steep-spectrum synchrotron emission is much stronger than the flat-spectrum free-free emission, so most SFGs have spectral indices $\alpha \equiv d \ln(S)/d \ln(\nu) \approx -0.7$ (Condon 1992).

Combining FIR and radio observations of RBGS galaxies adds value to both. Nearly all SFGs are optically thin to $\lambda = 60 \mu\text{m}$ dust emission, so the *IRAS* RBGS is the purest complete sample of star-forming galaxies in the local universe. The majority of RBGS galaxies are also bright optically, but a significant fraction of optically luminous galaxies have low star-formation rates (SFRs) (Condon et al. 2019) and galaxies with the highest SFRs are often too dusty to stand out in photographic catalogs. Aperture-synthesis radio observations can yield images with significantly higher angular resolution and smaller position errors, and unusually low FIR/radio flux-density ratios can reveal the presence of obscured AGNs (Condon et al. 2019). The radio and FIR morphologies of SFGs are similar, but the radio emission is blurred by cosmic-ray diffusion (Mur-

phy et al. 2008) and can reveal winds and outflows from galactic disks (Adebarh et al. 2013).

The most important new population in the *IRAS* RBGS is the subsample of ≈ 200 luminous infrared galaxies (LIRGs) defined by $L_{\text{IR}}(8-1000 \mu\text{m}) \geq 10^{11} L_{\odot}$, where $H_0 = 70 \text{ km s}^{-1} \text{ Mpc}^{-1}$ was used to calculate L_{IR} and $L_{\odot} \equiv 3.83 \times 10^{26} \text{ W}$ is the nominal bolometric luminosity of the Sun. A significant fraction of low-redshift LIRGs are merging systems containing nuclear starbursts and/or AGNs (Sanders & Mirabel 1996), and LIRGs at redshifts $z \gtrsim 1$ produced most of the stars in the universe today. The Great Observatories All-sky LIRG Survey (GOALS, Armus et al. 2009) is a comprehensive imaging and spectroscopic survey of RBGS LIRGs.

The “characteristic” infrared luminosity $L_{\text{IR}}^* \approx 10^{10.5} L_{\odot}$ (Sanders et al. 2003) of RBGS galaxies is a large fraction of their characteristic bolometric luminosity. In contrast, radio continuum emission is only an energetically insignificant tracer—the typical IR/radio luminosity ratios of SFGs are $> 10^5$ —making it vulnerable to contamination by potentially more luminous AGN emission.

To quantify the FIR/radio flux density ratio, Helou et al. (1985) defined the parameter

$$q \equiv \log \left[\frac{F_{\text{FIR}}/(3.75 \times 10^{12} \text{ Hz})}{S(1.4 \text{ GHz})} \right], \quad (1)$$

where $S(1.4 \text{ GHz})$ is the 1.4 GHz flux density in $\text{W m}^{-2} \text{ Hz}^{-1}$ and F_{FIR} is the far-infrared flux in W m^{-2} in the band of width $3.75 \times 10^{12} \text{ Hz}$ between $\lambda = 42.5 \mu\text{m}$ and $\lambda = 122.5 \mu\text{m}$ calculated from

$$F_{\text{FIR}} \equiv 1.26 \times 10^{-14} [2.58S(60 \mu\text{m}) + S(100 \mu\text{m})] \quad (2)$$

using infrared flux densities $S(60 \mu\text{m})$ and $S(100 \mu\text{m})$ in Jy. Typical values for SFGs are $S(100 \mu\text{m}) \approx 2S(60 \mu\text{m})$ and $q = 2.3$, making most RBGS galaxies with $S_{60 \mu\text{m}} \geq 5.24 \text{ Jy}$ radio sources with $S(1.4 \text{ GHz}) \gtrsim 40 \text{ mJy}$. The radio luminosities of RBGS galaxies with low star-formation rates are not diluted by cold “cirrus” dust emission in the diffuse interstellar medium heated by stars older than 30 Myr. In addition to being only a tracer, the synchrotron luminosity of an SFG depends on too many unmeasured parameters to be modeled quantitatively, so the theoretical foundation for the tight empirical FIR/radio correlation is weak.

The main drawback of the *IRAS* images is their limited angular resolution—half of the RBGS sources are unresolved by the $1.5' \times 4.5'$ response of *IRAS* (Neugebauer et al. 1984) detectors at $\lambda = 60 \mu\text{m}$, and the smallest galaxies that show structural features at *IRAS* resolution have blue isophotal angular diameters $\gtrsim 8'$ (Rice

et al. 1988). Only at radio wavelengths is the sensitivity of multi-element interferometers nearly immune to the quantum noise which adds $T \approx 50 \text{ K} \times (\nu/\text{THz})$ to the noise temperature of coherent amplifiers, allowing large radio arrays such as MeerKAT to achieve much higher angular resolution and astrometric accuracy than *IRAS*. Comparisons of higher-resolution *Spitzer* $\lambda = 70 \mu\text{m}$ images of the nearest ($D < 11.5 \text{ Mpc}$) galaxies with 1.4 GHz radio images show similar FIR and radio morphologies, and their small differences can usually be explained by cosmic-ray diffusion smoothing the radio images and by cirrus emission in the FIR images of quiescent SFGs (Murphy et al. 2008). Moreover, the mid-infrared “warm” dust has been shown to be a good tracer of the cold FIR (e.g., Cluver et al. 2017), which enables using higher resolution imaging from *Spitzer* and *WISE* that closer matches that of the radio interferometry.

This paper presents new MeerKAT images with FWHM resolution $\theta \approx 7.5''$ and rms fluctuations $\sigma \approx 20 \mu\text{Jy beam}^{-1}$ covering all 298 RBGS sources identified with external galaxies in the southern hemisphere (J2000 $\delta < 0$). The observations and imaging processes are described in Section 2. The resulting MeerKAT Atlas of 1.28 GHz continuum images is presented in Section 3. Table 3 lists the 1.28 GHz total flux densities of southern RBGS sources plus fitted source-component parameters (peak and integrated flux densities, deconvolved angular sizes, and J2000 positions). Section 4 summarizes the MeerKAT Atlas results and their significance.

The original RBGS catalog (Sanders et al. 2003) used $H_0 = 75 \text{ km s}^{-1} \text{ Mpc}^{-1}$ and $\Omega_m = 0.3$ to calculate absolute quantities in a Λ CDM universe. For comparison with the more frequently used $H_0 = 70 \text{ km s}^{-1} \text{ Mpc}^{-1}$, the distances in Table 2 should be multiplied by 1.071 and $\log(L/L_{\odot})$ should be increased by 0.060. This paper uses the spectral-index sign convention $\alpha \equiv +d \ln S / d \ln \nu$. Most SFGs have spectral indices near $\alpha = -0.7$, so $S(1.4 \text{ GHz}) \approx 0.94 S(1.28 \text{ GHz})$.

2. MEERKAT OBSERVATIONS AND IMAGING

Our observations were scheduled as two MeerKAT projects: (1) the director’s discretionary time project DDT-20200520-TM-01 with six observing runs in 2020 May and June plus (2) the “open time” project SCI-20210212-TJ-01 with eight runs in 2021 February and March. The 14 observing runs are labeled “A” through “N” and listed in Table 1 along with their starting dates, UTC time ranges, and calibration sources. Each run was ~ 8 hr long and cycled through five 3 min integrations on each of $\gtrsim 20$ RBGS targets passing near transit. The DDT project pioneered the

use of “snapshot” observations with MeerKAT to observe large numbers of sources quickly, as described in the SARAO science commissioning report “Snapshot Observations with MeerKAT” (Mauch et al. 2020a). Single pointing positions of the $\Theta_{1/2} = 68'$ FWHM MeerKAT primary beam were able to cover each of these five target groups: F02069–1022, F02071–1023, and F02072–1025; 09432–1405 and F09433–1408; 14214–1629 and 14216–1632; F14376–0004 and F14383–0006; and F23156–4238, F23161–4230, and F23165–4231.

A single complex gain (both amplitude and phase) calibrator was observed twice per hour throughout each run. In addition, the flux-density/bandpass calibrators J0408–6545 and/or PKS B1934–638 = J1939–6342 were observed with several 10 min scans in each run. Our flux-density scale is based on the Reynolds (1994) spectrum of PKS B1934–638 = J1939–6342:

$$\log(S) = -30.7667 + 26.4908(\log \nu) - 7.0977(\log \nu)^2 + 0.605334(\log \nu)^3, \quad (3)$$

where S is the flux density in Jy and ν is the frequency in MHz. A single 10 min scan of the polarization calibrator 3C 138 or 3C 286 was made when possible, and the resulting polarization calibration was applied to runs lacking scans on these polarization calibrators as described in Section 2.1.

The observed frequency range 856 to 1712 MHz was divided into 4096 spectral channels and the integration time was 8 s to minimize bandwidth and time smearing. Weak, irregular receiver response and strongly elliptical primary beams at the correlator band edges limit the useful frequency range to $880 \lesssim \nu(\text{MHz}) \lesssim 1670$ whose midpoint is $\nu \approx 1280$ MHz. All combinations of the linearly polarized feeds were correlated and recorded. Typically, more than 60 of the 64 MeerKAT antennas were operating during our observations.

2.1. Calibration

The 144 spectral channels on each end of the bandpass were deleted and the remaining channels were divided into 8 spectral windows for calibration purposes. Initial flagging and calibration were as described in Mauch et al. (2020b) and Cotton et al. (2020) using the *Obit* (Cotton 2008) software package. Channels containing persistent, strong interference were flagged. Parallel-hand calibration consisted of intermixed calibration and editing steps: after a first pass, the flagging was kept, the calibration tables were deleted, and the process was repeated. Calibration included group delay, band-

pass, and gain calibration. The bandpass calibrators J0408–6455 and PKS B1934–638 = J1939–6342 are so weakly polarized that they can be used to fix the gain ratios of the two orthogonally polarized feeds. Gain calibration subsequent to bandpass calibration used only Stokes I to preserve those gain ratios.

The polarization calibration for all runs included instrumental cross-hand delay and phase calibration based on the “DelayCal” calibration performed prior to the beginning of each observing run. Runs that included a polarization calibrator had instrumental polarization and residual cross-hand phases determined and applied to the data. The initial instrumental cross-hand delay calibration leaves sufficiently stable residuals that the calibration derived from a run with a polarization calibrator can be applied to another run without one.

2.2. Imaging Process

All pointings were imaged in Stokes I , Q , U , and V by the *Obit* task MFImage (Cotton et al. 2018). MFImage divides the sky into small flat facets to approximate the curvature of the sky and divides the data into spectral bins narrow enough that variations of antenna gain and sky brightness with frequency do not lower image quality. The spectral bins were imaged independently and CLEANed jointly.

Each pointing was fully imaged out to the first zero of the MeerKAT primary beam $72'$ from the pointing center. Outlying facets were added up to $90'$ from the pointing center to cover individual sources from the NVSS (Condon et al. 1998) or SUMSS catalogs (Mauch et al. 2003) having flux densities $S > 1$ mJy after attenuation by the primary beam. The frequency bins have 0.05 maximum fractional bandwidth and the baseline-dependent time averaging was constrained to neither exceed 30 s nor lower any amplitude in the field of view by more than 1%. An *AIPS/Obit* Robust factor $R = -1.5$ was used to produce nearly circular Gaussian restoring beams with FWHM major and minor diameters $\theta_M \approx \theta_m \approx 7''.5$. Because the Rayleigh-Jeans brightness temperature corresponding to a peak flux density S_P is

$$\left(\frac{T_b}{K} \right) \approx 0.26 \left(\frac{S_P}{20 \mu\text{Jy beam}^{-1}} \right) \times \left(\frac{7''.5}{\theta_M} \right) \left(\frac{7''.5}{\theta_m} \right) \left(\frac{1.28 \text{ GHz}}{\nu} \right)^2, \quad (4)$$

an rms image fluctuation $\sigma_n \approx 20 \mu\text{Jy beam}^{-1}$ is sufficient for detecting most optically selected SFGs, which have median face-on disk brightness temperature $\langle T_b \rangle \gtrsim 1$ K at $\nu = 1.28$ GHz (Hummel 1981). At the median

Table 1. MeerKAT Observation Log

Run	Start Date	UTC Time Range	Calibration Sources
A	2020 May 29	19:47–27:45	3C 286, J1830–3602, J1939–6342
B	2020 Jun. 11	14:46–22:44	J0408–6545, 3C 286, 1424–4913, J1939–6342
C	2020 Jun. 13	02:08–10:00	J0408–6545, J0440–4333
D	2020 Jun. 15	23:31–31:25	3C 138, J1939–6342
E	2020 Jun. 20	04:48–14:44	J0408–6545, J0616–3456
F	2020 Jun. 21	12:01–20:00	J0408–6545, J1154–3505, 3C 286
G	2021 Feb. 20	00:33–07:35	3C 296, J1939–6342
H	2021 Feb. 21	09:03–17:05	J0408–6545, 3C 138, J1939–6342
I	2021 Feb. 24	14:38–22:29	J0408–6545, J0609–1542, 3C 138
J	2021 Feb. 24	22:32–30:41	J0408–6545, J1311–2216, 3C 286, J1939–6342
K	2021 Feb. 28	09:08–16:10	J0408–6545, 3C 138, J1939–6342
L	2021 Feb. 28	21:57–29:29	J0408–6545, J1154–3505, 3C 286, J1939–6342
M	2021 Mar. 05	11:35–19:25	J0240–2309, J0408–6545, 3C 138
N	2021 Mar. 23	17:02–24:40	J0408–6545, J1120–2508, 3C 286, J1939–6342

angular-size distance $D_A = D_C/(1+z) \approx 50$ Mpc of RBGS galaxies (Sanders et al. 2003), $7.^{\circ}5 = 1.8$ kpc.

Each run used a single complex-gain calibrator for target fields separated by up to a radian on the sky, so the external phase calibration is not always very accurate. In order to mitigate this, a relatively complicated self-calibration scheme was used. All pointings use three cycles of 30 s phase-only self calibration preceded by CLEANs reaching residual peak flux densities of 10, 2, and 0.5 mJy beam $^{-1}$. This helps prevent artifacts from the initial calibration from corrupting the self-calibration model. For fields with peak flux densities in excess of 1 Jy beam $^{-1}$, a scan-averaged amplitude and phase self calibration was applied. Sources with peaks in excess of 0.15 Jy beam $^{-1}$ were centered in their own facets to facilitate CLEANing and improve the image dynamic range.

CLEAN windowing used the MFImage “autoWindow” facility. Final CLEANing in Stokes I with a loop gain of 0.05 proceeded to a residual peak flux density $S_p = 100 \mu\text{Jy beam}^{-1}$ or a maximum of 50,000 components. Stokes Q and U images were CLEANed to a depth of $50 \mu\text{Jy beam}^{-1}$ or a maximum of 8,000 components, and Stokes V CLEANing was stopped after reaching $50 \mu\text{Jy beam}^{-1}$ or a maximum of 1,000 components.

2.3. Imaging Data Products

Two of the 14 frequency planes were totally blanked to eliminate strong radio-frequency interference. MFImage produced CLEAN restored images in the 12 remaining frequency planes. Each image plane was divided by

the primary beam attenuation pattern as described in Mauch et al. (2020b) to yield “on sky” brightnesses. A flux density and then a flux-density plus spectral index were fitted in each pixel. If the higher-order fit did not increase χ^2 by more than 1.5, the spectral index was kept; otherwise, a default spectral index $\alpha = -0.6$ was used. The limited frequency range does not allow usefully accurate spectral curvature fits. The region within $20'$ of each target galaxy was extracted for further analysis.

Off-source brightness fluctuations in the Stokes I images are produced by a combination of thermal noise, confusion by faint sources overlapping within the synthesized beams, and residual sidelobes of imperfectly calibrated strong sources. We estimated the rms brightness fluctuation in the central $16' \times 16'$ square of each image using the *AIPS* task IMEAN, which fits a Gaussian to the peak of the pixel brightness distribution. The rms σ of that Gaussian fit excludes the long tail of very bright pixels on individual sources. Figure 1 shows the normalized distribution of σ for our MeerKAT images. The rms thermal noise is $\sigma_n \approx 15 \mu\text{Jy beam}^{-1}$ and the rms confusion caused by very faint sources is $\sigma_c \approx 2 \mu\text{Jy beam}^{-1}$. The quietest images have $\sigma \approx \sigma_n$ and the typical image has $\sigma \lesssim 20 \mu\text{Jy beam}^{-1}$. Significantly larger values of σ occur in fields containing residual sidelobes of strong ($S \gtrsim 200$ mJy) target or background sources. The snapshot image dynamic range (ratio of image peak flux density to σ) is typically between $10^4 : 1$ and $3 \times 10^4 : 1$.

The final step in constructing the Atlas Stokes I images was correcting for the negative “bowl” that results from incomplete CLEANing of an interferometric im-

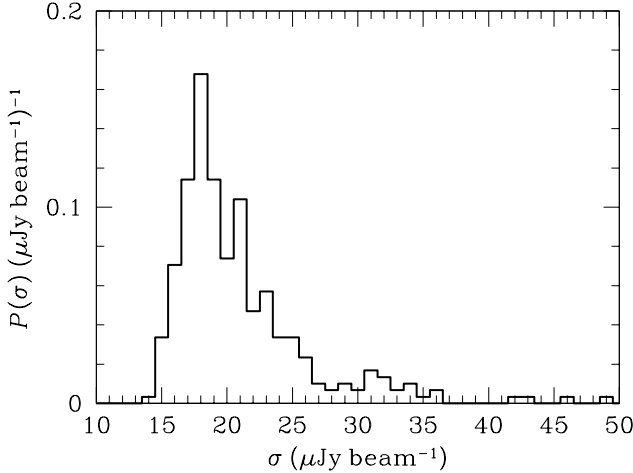


Figure 1. This histogram shows the probability distribution $P(\sigma)$ of rms brightness fluctuations σ in the central $16' \times 16'$ squares of our MeerKAT RBGS images. The long tail is caused by sidelobes from target nuclei or background AGNs brighter than $S_p \sim 200 \text{ mJy beam}^{-1}$.

age lacking zero-spacing data. We measured the median brightness in a large source-free region surrounding each target and subtracted that median brightness from the image. Most bowl depths were only -1 or $-2 \mu\text{Jy beam}^{-1}$ and there are ≈ 57 beam solid angles per arcmin^2 , so the corrections are small and add $\lesssim 0.1 \text{ mJy}$ to the total flux densities of most target galaxies.

Linear polarization was analyzed as described in Cottet et al. (2020) using a simple rotation-measure (RM) analysis to derive the intrinsic angle of the polarized emission. RMAs and electric-vector position angles corrected to zero wavelength were derived from a search in RM space. The RM giving the highest polarized intensity $P = (Q^2 + U^2)^{1/2}$ was taken to be the actual RM, the highest P as the polarized intensity, and the polarization angle of the RM-corrected $Q + iU$ as the electric-vector position angle corrected to zero wavelength. Stokes Q and U images were extracted in the same regions as Stokes I . The rms image noise in the Stokes Q and U images is close to the thermal noise, $\sigma_n \approx 15 \mu\text{Jy beam}^{-1}$.

Cropped MeerKAT images in FITS format covering all 298 southern RBGS sources are available via <https://doi.org/10.48479/dnt7-6q05> as a single 221 Mbyte

compressed file, and individual images are available as ~ 1 Mbyte uncompressed FITS files.

3. THE MEERKAT 1.28 GHZ ATLAS OF SOUTHERN RBGS SOURCES

3.1. IRAS data

There are 300 RBGS sources south of J2000 declination $\delta = 0^\circ$. We observed all but the two Magellanic Clouds because they are only satellites of our Galaxy. Our Galaxy and its satellites are not external galaxies representative of the universe as a whole, unbiased by our location. The remaining 298 are listed in Table 2, which is a subset of Sanders et al. (2003, table 1). There is one row per *IRAS* source listing:

Column (1).—Our infrared source index number N running from 1 through 298 for easier comparison with other tables and lists in this paper.

Column (2).—The most common galaxy name(s).

Column (3).—The *IRAS* source name.

Columns (4)–(5).—The *IRAS* J2000 right ascension α and declination δ .

Column (6).—RBGS flux density at $\lambda = 12 \mu\text{m}$ (Jy).

Column (7).—RBGS flux density at $\lambda = 25 \mu\text{m}$ (Jy).

Column (8).—RBGS flux density at $\lambda = 60 \mu\text{m}$ (Jy).

Column (9).—RBGS flux density at $\lambda = 100 \mu\text{m}$ (Jy).

Column (10).—Comoving distance D_C (Mpc) calculated by Sanders et al. (2003) for a flat universe with $H_0 = 75 \text{ km s}^{-1} \text{ Mpc}^{-1}$. For $H_0 = 70 \text{ km s}^{-1} \text{ Mpc}^{-1}$, this listed D_C should be multiplied by $75/70 \approx 1.07$.

Column (11).—Logarithm of the absolute IR [$8 < \lambda(\mu\text{m}) < 1000$] luminosity L_{IR}/L_\odot in units of the solar bolometric luminosity $L_\odot = 3.83 \times 10^{26} \text{ W}$. The infrared fluxes F_{IR} in W m^{-2} were extrapolated from *IRAS* flux densities in Jy using (Sanders & Mirabel 1996)

$$F_{\text{IR}} = 1.8 \times 10^{-14} (13.48 S_{12 \mu\text{m}} + 5.16 S_{25 \mu\text{m}} + 2.58 S_{60 \mu\text{m}} + S_{100 \mu\text{m}}). \quad (5)$$

The corresponding luminosities are $L_{\text{IR}} = 4\pi D_L^2 F_{\text{IR}}$, where $D_L = (1+z)D_C$ is the bolometric luminosity distance.

Column (12).—An asterisk indicates the source is one of the 94 southern sources in the GOALS (Armus et al. 2009) sample of LIRGs defined by $\log(L_{\text{IR}}/L_\odot) \geq 11.0$ calculated using $H_0 = 70 \text{ km s}^{-1} \text{ Mpc}^{-1}$ instead of $H_0 = 75 \text{ km s}^{-1} \text{ Mpc}^{-1}$.

Table 2. The Southern RBGS Sample: *IRAS* Data

Index	Common N	<i>IRAS</i> Name	α (J2000)	δ (Jy)	$S_{12\mu\text{m}}$ (Jy)	$S_{25\mu\text{m}}$ (Jy)	$S_{60\mu\text{m}}$ (Jy)	$S_{100\mu\text{m}}$ (Jy)	D_C (Mpc)	$\log(L_{\text{IR}}/L_\odot)$	GOALS
		Name	(4)	(5)	(6)	(7)	(8)	(9)	(10)	(11)	(12)
		(3)									
001	NGC 0034	F00085–1223	00 11 06.6	–12 06 27	0.35	2.39	17.05	16.86	77.60	11.44	*
002	NGC 0055	NGC 0055	00 14 54.5	–39 11 19	1.34	6.25	77.00	174.09	3.10	9.36	
003	MCG -02-01-051/2	F00163–1039	00 18 51.4	–10 22 33	0.28	1.20	7.48	9.66	105.76	11.41	*
004	NGC 0134	F00278–3331	00 30 21.6	–33 14 38	2.35	2.59	22.65	58.87	15.90	10.37	
005	ESO 079-G003	F00298–6431	00 32 02.0	–64 15 14	0.42	0.88	7.05	17.41	35.31	10.51	
006	NGC 0150	F00317–2804	00 34 16.2	–27 48 10	0.66	1.66	9.66	17.72	16.20	9.95	
007	NGC 0157	F00322–0840	00 34 46.0	–08 23 53	1.61	2.17	17.93	42.43	21.92	10.52	
008	ESO 350-IG038	F00344–3349	00 36 52.0	–33 33 19	0.52	2.51	6.88	5.04	81.20	11.22	*
009	NGC 0174	F00345–2945	00 36 58.4	–29 28 45	0.41	1.27	11.36	19.77	47.28	10.90	
010	NGC 0232	F00402–2349	00 42 46.5	–23 33 31	0.36	1.28	10.05	17.14	79.23	11.30	*
011	NGC 0247	F00446–2101	00 47 06.0	–20 45 48	0.14	0.89	8.73	23.50	3.10	8.45	
012	NGC 0253	F00450–2533	00 47 33.1	–25 17 15	41.04	154.67	967.81	1288.15	3.10	10.44	
013	NGC 0289	F00502–3128	00 52 42.8	–31 12 19	0.45	0.60	5.47	16.90	21.60	10.03	
014	NGC 0300	NGC 0300	00 54 52.9	–37 41 09	0.90	1.96	15.30	48.04	2.00	8.39	
015	NGC 0337	F00573–0750	00 59 49.6	–07 34 52	0.24	0.76	9.07	20.11	21.59	10.13	
016	IC 1623A/B	F01053–1746	01 07 46.3	–17 30 32	1.03	3.65	22.93	31.55	78.57	11.65	*
017	MCG -03-04-014	F01076–1707	01 10 08.5	–16 51 14	0.34	0.90	7.25	10.33	136.17	11.63	*
018	ESO 244-G012	F01159–4443	01 18 08.6	–44 27 40	0.39	1.95	9.27	11.76	90.96	11.39	*
019	NGC 0613	F01319–2940	01 34 17.8	–29 25 10	2.25	4.32	27.38	59.21	14.98	10.37	
020	ESO 353-G020	F01325–3623	01 34 49.4	–36 08 25	0.37	0.71	7.17	15.54	63.37	11.00	*
021	NGC 0625	F01329–4141	01 35 05.8	–41 26 17	0.20	1.30	5.73	8.63	4.46	8.57	
022	ESO 297-G011/012	F01341–3735	01 36 24.7	–37 19 56	0.37	1.55	7.77	12.90	67.88	11.09	*
023	IRAS F01364–1042	F01364–1042	01 38 52.6	–10 27 15	< 0.16	0.44	6.62	6.88	188.37	11.76	*
024	NGC 0643B	F01384–7515	01 39 12.9	–75 00 40	0.32	0.84	7.36	13.76	54.59	10.85	
025	NGC 0701	F01486–0956	01 51 04.5	–09 42 04	0.62	0.67	6.17	14.90	19.87	9.98	
026	NGC 0835	F02069–1022	02 09 23.8	–10 08 13	0.36	0.50	5.31	12.60	52.90	10.74	
027	NGC 0838	F02071–1023	02 09 38.8	–10 08 46	0.68	1.88	11.41	19.94	50.13	11.00	*
028	NGC 0839	F02072–1025	02 09 42.9	–10 11 03	0.52	2.27	11.67	13.03	51.10	10.97	
029	NGC 0873	F02141–1134	02 16 33.2	–11 20 50	0.44	0.69	5.81	12.86	52.45	10.77	
030	NGC 0908	F02207–2127	02 23 05.3	–21 13 58	1.74	2.21	17.54	52.35	15.75	10.27	
031	NGC 0922	F02228–2500	02 25 04.2	–24 47 21	0.33	0.74	5.53	9.68	40.57	10.48	
032	NGC 0958	F02281–0309	02 30 43.0	–02 56 18	0.62	0.94	5.85	15.08	76.36	11.17	*
033	NGC 0986	F02315–3915	02 33 34.3	–39 02 42	1.42	3.65	25.06	49.88	26.43	10.78	
034	NGC 1022	F02360–0653	02 38 31.8	–06 40 40	0.71	3.28	19.71	27.33	19.33	10.35	
035	NGC 1068	F02401–0013	02 42 41.4	–00 00 45	39.84	87.57	196.37	257.37	13.70	11.27	*
036	NGC 1083	F02433–1534	02 45 40.0	–15 21 30	0.31	0.78	7.68	13.57	53.46	10.84	
037	NGC 1084	F02435–0747	02 45 59.7	–07 34 41	1.96	3.20	29.41	58.64	18.61	10.54	
038	NGC 1087	02438–0042	02 46 25.1	–00 29 53	0.97	1.41	12.16	27.98	20.05	10.26	

Table 2 *continued*

Table 2 (*continued*)

Index	Common	<i>IRAS</i>	α	δ	$S_{12\mu\text{m}}$	$S_{25\mu\text{m}}$	$S_{60\mu\text{m}}$	$S_{100\mu\text{m}}$	D_{C}	$\log(L_{\text{IR}}/L_{\odot})$	GOALS
<i>N</i>	Name	Name	(J2000)		(Jy)	(Jy)	(Jy)	(Jy)	(Mpc)	(11)	(12)
(1)	(2)	(3)	(4)	(5)	(6)	(7)	(8)	(9)	(10)		
039	NGC 1097	F02441–3029	02 46 18.7	–30 16 29	2.96	7.30	53.35	104.79	16.80	10.71	
040	NGC 1187	F03004–2303	03 02 37.9	–22 52 00	0.91	1.85	11.75	26.44	18.32	10.18	
041	NGC 1204	F03022–1232	03 04 40.5	–12 20 26	0.25	1.10	7.33	10.18	58.51	10.88	
042	NGC 1222	F03064–0308	03 08 57.3	–02 57 16	0.50	2.28	13.06	15.41	32.26	10.60	
043	NGC 1232	F03075–2045	03 09 45.8	–20 34 32	0.88	1.32	8.37	28.47	22.13	10.28	
044	NGC 1266	F03135–0236	03 16 01.7	–02 25 34	0.25	1.20	13.13	16.89	28.86	10.46	
045	NGC 1313	F03176–6640	03 18 16.7	–66 29 30	0.89	2.48	30.71	63.14	4.00	9.18	
046	NGC 1309	F03197–1534	03 22 07.1	–15 23 53	0.32	0.63	6.16	14.68	28.11	10.24	
047	NGC 1326	F03220–3638	03 23 55.9	–36 27 52	0.52	0.93	8.01	13.99	16.13	9.84	
048	IC 1953	F03314–2138	03 33 41.7	–21 28 43	0.21	0.96	8.81	11.97	24.64	10.17	
049	NGC 1365	F03316–3618	03 33 36.5	–36 08 23	5.12	14.28	94.31	165.67	17.93	11.00	*
050	NGC 1377	F03344–2103	03 36 38.2	–20 54 08	0.56	1.93	7.43	5.95	23.66	10.13	
051	NGC 1386	F03348–3609	03 36 45.5	–35 59 58	0.52	1.46	5.92	9.55	10.90	9.42	
052	NGC 1385	F03353–2439	03 37 28.8	–24 29 59	1.17	2.00	17.23	36.03	15.90	10.18	
053	NGC 1406	F03373–3129	03 39 23.2	–31 19 20	1.00	1.38	12.87	27.49	18.98	10.22	
054	NGC 1415	F03387–2243	03 40 56.8	–22 33 53	0.53	0.55	5.68	12.27	20.91	9.96	
055	NGC 1421	F03401–1338	03 42 27.7	–13 29 23	0.80	1.40	10.95	22.62	21.20	10.25	
056	NGC 1448	F03428–4448	03 44 32.1	–44 38 41	1.10	1.44	10.32	32.43	11.47	9.78	
057	NGC 1482	F03524–2038	03 54 39.8	–20 30 07	1.55	4.68	33.36	46.73	25.09	10.80	
058	NGC 1511	F03594–6746	03 59 37.4	–67 38 06	1.21	3.25	25.38	40.75	16.33	10.32	
059	NGC 1532	F04101–3300	04 12 01.2	–32 53 11	1.00	1.12	9.63	30.61	15.51	10.01	
060	ESO 420-G013	F04118–3207	04 13 50.1	–32 00 24	0.95	2.22	13.66	20.88	47.60	11.02	*
061	NGC 1546	04134–5611	04 14 29.6	–56 04 13	0.46	0.73	5.40	20.05	15.93	9.80	
062	IC 2056	F04155–6019	04 16 24.2	–60 12 26	0.49	0.76	6.06	12.67	13.75	9.62	
063	NGC 1559	F04170–6254	04 17 37.4	–62 46 59	1.84	3.05	30.24	61.20	12.69	10.21	
064	NGC 1566	F04188–5503	04 19 59.8	–54 56 06	1.91	3.02	22.53	58.05	19.10	10.51	
065	ESO 550-IG025	F04191–1855	04 21 19.6	–18 48 45	0.22	0.51	5.69	9.47	126.43	11.45	*
066	NGC 1572	F04210–4042	04 22 42.3	–40 36 03	0.23	0.80	8.03	16.81	81.50	11.24	*
067	NGC 1614	F04315–0840	04 34 00.1	–08 34 46	1.38	7.50	32.12	34.32	62.61	11.60	*
068	ESO 485-G003	F04370–2416	04 39 06.5	–24 11 02	0.34	0.69	6.07	11.34	60.51	10.87	
069	NGC 1637	F04389–0257	04 41 29.6	–02 51 26	0.65	1.47	6.61	15.71	10.16	9.46	
070	NGC 1672	F04449–5920	04 45 42.7	–59 14 48	2.47	5.25	41.21	77.92	16.82	10.59	
071	ESO 203-IG001	F04454–4838	04 46 50.3	–48 33 31	< 0.05	0.45	5.86	5.38	208.86	11.79	*
072	NGC 1667	F04461–0624	04 48 37.7	–06 19 12	0.63	0.71	6.27	14.92	60.51	10.96	
073	MCG -05-12-006	F04502–3304	04 52 06.8	–32 59 24	0.22	1.21	8.15	9.85	75.05	11.12	*
074	IC 0398	F04557–0751	04 58 12.4	–07 46 50	0.21	0.55	5.63	11.03	50.29	10.66	
075	NGC 1720	F04569–0756	04 59 19.9	–07 51 34	0.31	0.77	7.00	13.30	55.68	10.85	
076	NGC 1792	F05035–3802	05 05 13.7	–37 58 46	3.18	4.31	35.16	86.15	12.54	10.33	
077	NGC 1797	F05053–0805	05 07 44.2	–08 01 09	0.33	1.35	9.56	12.76	59.13	11.00	*

Table 2 *continued*

Table 2 (*continued*)

Index	Common	<i>IRAS</i>	α	δ	$S_{12\mu\text{m}}$	$S_{25\mu\text{m}}$	$S_{60\mu\text{m}}$	$S_{100\mu\text{m}}$	D_C	$\log(L_{\text{IR}}/L_\odot)$	GOALS
<i>N</i>	Name	Name	(J2000)		(Jy)	(Jy)	(Jy)	(Jy)	(Mpc)	(11)	(12)
(1)	(2)	(3)	(4)	(5)	(6)	(7)	(8)	(9)	(10)		
078	NGC 1808	F05059–3734	05 07 42.3	–37 30 48	5.40	17.00	105.55	141.76	12.61	10.71	
079	NGC 1832	F05097–1544	05 12 03.1	–15 41 17	0.58	0.86	7.35	17.77	26.24	10.28	
080	IRAS F05187–1017	F05187–1017	05 21 06.3	–10 14 45	< 0.08	0.19	5.39	8.04	111.81	11.23	*
081	IRAS F05189–2524	F05189–2524	05 21 01.4	–25 21 46	0.74	3.47	13.25	11.84	168.64	12.11	*
082	NGC 1964	F05312–2158	05 33 21.8	–21 56 44	0.69	1.02	9.17	23.48	18.65	10.09	
083	NGC 2076	F05445–1648	05 46 47.9	–16 46 58	0.71	0.76	7.03	20.46	29.48	10.41	
084	NGC 2139	F05590–2340	06 01 07.2	–23 40 25	0.28	0.86	7.05	14.05	25.11	10.16	
085	ESO 121-G006	F06070–6147	06 07 29.5	–61 48 28	0.58	0.68	6.11	15.20	14.52	9.70	
086	IRAS F06076–2139	F06076–2139	06 09 45.1	–21 40 22	0.06	0.63	6.43	8.47	148.80	11.59	*
087	NGC 2207/IC 2163	F06142–2121	06 16 22.9	–21 22 20	1.37	2.45	17.55	40.85	36.93	10.96	
088	UGCA 127	F06185–0828	06 20 56.9	–08 29 42	1.41	1.62	17.61	39.38	10.19	9.82	
089	UGCA 128	F06189–2001	06 21 05.4	–20 02 53	0.54	0.93	5.38	11.90	27.28	10.21	
090	NGC 2221	F06194–5733	06 20 16.0	–57 34 43	0.30	0.56	6.41	13.94	33.83	10.39	
091	ESO 005-G004	F06218–8636	06 05 36.5	–86 37 53	0.61	0.81	7.48	19.25	22.36	10.16	
092	ESO 255-IG007	F06259–4708	06 27 21.1	–47 10 38	0.32	1.42	9.05	11.85	155.32	11.84	*
093	ESO 557-G002	F06295–1735	06 31 46.3	–17 37 15	0.17	0.86	7.42	10.50	85.61	11.19	*
094	NGC 2280	F06428–2735	06 44 50.0	–27 38 23	0.68	0.85	7.11	18.78	21.54	10.13	
095	IRAS 06478–1111	06478–1111	06 50 11.2	–11 15 14	0.41	0.66	5.96	8.34	36.36	10.39	
096	IRAS F06592–6313	F06592–6313	06 59 40.3	–63 17 53	0.14	0.78	5.74	7.52	94.76	11.17	*
097	AM 0702-601	F07027–6011	07 03 27.5	–60 16 05	0.43	1.37	6.70	9.26	127.33	11.58	*
098	ESO 491-G020/021	07077–2729	07 09 47.0	–27 34 10	0.91	2.70	15.23	22.85	41.10	10.93	
099	ESO 492-G002	07096–2637	07 11 40.7	–26 42 19	0.41	0.79	7.94	14.88	36.22	10.53	
100	NGC 2369	F07160–6215	07 16 37.7	–62 20 35	0.74	2.20	20.35	38.31	44.02	11.10	*
101	ESO 428-G023	07202–2908	07 22 10.7	–29 14 13	0.45	1.36	9.94	17.69	42.07	10.76	
102	NGC 2397	F07214–6854	07 21 19.5	–69 00 02	0.73	1.08	8.48	19.18	16.08	9.92	
103	ESO 428-G028	07216–2957	07 23 38.3	–30 03 08	0.45	0.78	6.10	14.82	31.08	10.35	
104	IRAS 07251–0248	07251–0248	07 27 37.5	–02 54 55	< 0.07	0.66	6.49	6.35	343.74	12.32	*
105	NGC 2442	F07365–6924	07 36 25.9	–69 31 17	1.62	1.83	14.85	46.61	17.33	10.30	
106	ESO 163-G011/010	F07369–5504	07 38 04.3	–55 11 27	0.40	0.75	6.18	13.27	38.07	10.50	
107	ESO 209-G009	F07568–4942	07 58 14.9	–49 51 09	0.87	1.29	12.09	31.84	11.81	9.81	
108	NGC 2525	F08032–1117	08 05 37.9	–11 25 40	0.68	0.89	7.31	16.83	22.69	10.16	
109	NGC 2566	08166–2520	08 18 45.6	–25 29 59	1.26	4.03	24.33	37.23	22.43	10.60	
110	NGC 2613	F08311–2248	08 33 23.2	–22 58 28	1.05	1.32	7.48	25.86	20.18	10.18	
111	IRAS 08355–4944	08355–4944	08 37 02.3	–49 54 32	0.64	2.27	9.44	8.02	107.50	11.56	*
112	ESO 432-IG006	08424–3130	08 44 27.6	–31 41 41	0.58	0.84	6.48	9.31	68.55	11.02	*
113	NGC 2665	F08437–1907	08 46 00.3	–19 18 08	0.29	1.09	6.43	9.62	24.35	10.08	
114	ESO 563-G028	F08485–2146	08 50 45.1	–21 57 45	0.36	0.81	8.21	15.84	36.31	10.54	
115	ESO 60-IG016	F08520–6850	08 52 31.1	–69 01 59	0.15	0.73	5.71	6.12	186.88	11.76	*
116	NGC 2706	F08536–0222	08 56 12.2	–02 33 47	0.56	0.59	6.64	14.01	24.36	10.15	

Table 2 *continued*

Table 2 (*continued*)

Index	Common	<i>IRAS</i>	α	δ	$S_{12\mu\text{m}}$	$S_{25\mu\text{m}}$	$S_{60\mu\text{m}}$	$S_{100\mu\text{m}}$	D_C	$\log(L_{\text{IR}}/L_\odot)$	GOALS
<i>N</i>	Name	Name	(J2000)		(Jy)	(Jy)	(Jy)	(Jy)	(Mpc)	(11)	(12)
(1)	(2)	(3)	(4)	(5)	(6)	(7)	(8)	(9)	(10)		
117	ESO 564-G011	F09004–2031	09 02 45.9	–20 43 28	0.52	1.32	8.95	11.41	36.73	10.57	
118	IRAS 09022–3615	09022–3615	09 04 12.8	–36 27 02	0.20	1.19	11.64	11.08	238.84	12.26	*
119	UGCA 150	F09083–0841	09 10 49.5	–08 53 36	0.64	0.73	6.03	20.65	26.85	10.30	
120	IRAS F09111–1007	F09111–1007	09 13 37.6	–10 19 28	0.11	0.74	6.75	10.68	218.20	12.00	*
121	ESO 126-G002	09122–6034	09 13 30.2	–60 47 24	0.54	2.04	11.61	15.39	37.25	10.70	
122	ESO 091-G016	09369–6315	09 38 13.6	–63 29 12	0.31	0.79	6.63	10.11	26.56	10.15	
123	NGC 2992	09432–1405	09 45 42.0	–14 19 35	0.63	1.38	7.51	17.22	33.15	10.52	
124	NGC 2993	F09433–1408	09 45 47.3	–14 21 58	0.63	1.61	10.58	23.07	34.69	10.67	
125	NGC 3059	F09496–7341	09 50 08.1	–73 55 24	1.06	1.62	13.52	30.51	14.24	10.00	
126	IC 2522	F09529–3253	09 55 07.3	–33 08 04	0.43	0.64	6.47	18.06	41.16	10.63	
127	NGC 3095	F09578–3118	10 00 06.2	–31 33 15	0.40	1.00	8.33	16.22	36.86	10.57	
128	NGC 3110	F10015–0614	10 04 02.7	–06 28 35	0.59	1.13	11.28	22.27	73.48	11.31	*
129	ESO 374-IG032	F10038–3338	10 06 04.2	–33 53 04	0.28	1.21	9.79	9.02	141.58	11.73	*
130	NGC 3125	F10042–2941	10 06 32.3	–29 56 06	0.31	0.74	5.33	6.67	9.39	9.15	
131	IC 2554	10075–6647	10 08 50.4	–67 01 53	1.10	2.71	16.96	34.84	15.72	10.18	
132	NGC 3175	F10124–2837	10 14 42.9	–28 52 25	1.06	1.67	13.70	31.49	13.45	9.96	
133	ESO 500-G034	F10221–2318	10 24 32.4	–23 33 17	0.38	1.43	10.46	16.01	52.10	10.94	
134	ESO 317-G023	F10225–3903	10 24 43.4	–39 18 29	0.34	0.89	13.83	23.08	37.69	10.74	
135	NGC 3256	F10257–4339	10 27 52.4	–43 54 25	3.57	15.69	102.63	114.31	35.35	11.56	*
136	NGC 3263	F10270–4351	10 29 12.3	–44 07 13	0.53	0.91	8.59	19.00	38.79	10.66	
137	NGC 3278	F10293–3941	10 31 35.7	–39 57 25	0.59	0.91	7.10	14.66	38.41	10.59	
138	NGC 3281	F10295–3435	10 31 52.1	–34 51 14	0.91	2.63	6.73	7.89	42.91	10.73	
139	ESO 264-G036	F10409–4556	10 43 07.0	–46 12 43	0.36	0.67	6.07	13.37	100.50	11.35	*
140	ESO 264-G057	F10567–4310	10 59 02.4	–43 26 33	0.34	0.81	5.69	12.16	75.74	11.08	*
141	ESO 093-G003	10574–6603	10 59 22.8	–66 19 23	0.67	1.00	10.05	17.89	22.07	10.21	
142	NGC 3508	F11005–1601	11 03 00.1	–16 17 23	0.52	0.91	6.82	13.90	56.26	10.90	
143	NGC 3511	F11009–2249	11 03 24.2	–23 05 15	1.03	0.83	8.98	21.87	13.60	9.82	
144	ESO 265-G007	F11055–4615	11 07 48.8	–46 31 38	0.54	0.84	6.45	17.78	11.66	9.55	
145	ESO 215-G031	F11082–4849	11 10 34.7	–49 06 05	0.33	0.72	5.38	10.12	32.40	10.29	
146	NGC 3568	F11084–3710	11 10 50.4	–37 27 05	0.93	1.05	8.03	15.95	30.06	10.45	
147	NGC 3597	F11122–2327	11 14 40.9	–23 43 33	0.67	2.18	12.84	16.21	48.31	10.97	
148	NGC 3620	F11143–7556	11 16 04.1	–76 12 54	1.29	4.74	45.75	67.17	19.66	10.70	
149	NGC 3621	F11158–3232	11 18 16.7	–32 48 47	3.53	4.44	29.32	77.34	6.64	9.74	
150	CGCG 011-076	F11186–0242	11 21 13.3	–02 59 08	0.48	0.76	5.85	9.18	106.27	11.37	*
151	NGC 3672	F11224–0931	11 25 01.6	–09 47 34	1.01	0.95	9.23	25.69	27.70	10.47	
152	ESO 319-G022	F11255–4120	11 27 56.1	–41 37 06	0.16	0.95	7.68	9.52	72.26	11.04	*
153	NGC 3717	F11290–3001	11 31 31.2	–30 18 24	0.85	1.32	11.92	26.04	21.39	10.29	
154	NGC 3732	F11316–0934	11 34 13.4	–09 50 40	0.25	0.71	5.36	7.75	25.08	10.01	
155	NGC 3882	11436–5606	11 46 04.0	–56 23 12	1.51	2.67	19.84	37.38	20.62	10.47	

Table 2 *continued*

Table 2 (*continued*)

Index	Common	<i>IRAS</i>	α	δ	$S_{12\mu\text{m}}$	$S_{25\mu\text{m}}$	$S_{60\mu\text{m}}$	$S_{100\mu\text{m}}$	D_C	$\log(L_{\text{IR}}/L_\odot)$	GOALS
<i>N</i>	Name	Name	(J2000)		(Jy)	(Jy)	(Jy)	(Jy)	(Mpc)	(11)	(12)
(1)	(2)	(3)	(4)	(5)	(6)	(7)	(8)	(9)	(10)		
156	NGC 3885	F11442–2738	11 46 45.1	–27 55 10	0.57	1.47	11.89	16.25	22.93	10.27	
157	NGC 3887	F11445–1634	11 47 04.0	–16 51 00	0.59	0.67	5.84	16.81	16.07	9.80	
158	ESO 320-G030	F11506–3851	11 53 12.0	–39 07 54	0.53	2.28	34.38	46.28	37.70	11.10	*
159	NGC 3955	F11514–2253	11 53 57.5	–23 09 52	1.05	1.31	8.34	17.56	19.78	10.12	
160	NGC 3981	F11535–1937	11 56 07.1	–19 53 49	0.65	0.84	7.14	20.72	23.37	10.21	
161	NGC 4027	F11569–1859	11 59 28.8	–19 15 45	0.90	1.12	12.24	27.78	22.84	10.36	
162	NGC 4030	F11578–0049	12 00 23.8	–01 06 03	1.35	2.30	18.49	50.92	24.50	10.64	
163	NGC 4038/9	F11593–1836	12 01 55.1	–18 52 43	1.94	6.54	45.16	87.09	21.54	10.84	
164	ESO 440-IG058	F12043–3140	12 06 53.0	–31 57 08	0.20	0.76	7.44	12.63	100.48	11.36	*
165	ESO 267-G030	F12115–4656	12 14 12.6	–47 13 37	0.35	0.66	5.61	11.06	88.67	11.19	*
166	IRAS 12116–5615	12116–5615	12 14 21.4	–56 32 32	0.35	1.12	9.78	12.95	115.68	11.59	*
167	ESO 380-G001	F12121–3513	12 14 44.2	–35 30 31	0.38	1.92	11.48	18.81	30.92	10.54	
168	NGC 4219	F12138–4302	12 16 27.1	–43 19 26	0.93	1.91	14.08	36.78	22.58	10.44	
169	NGC 4304	F12196–3312	12 22 14.6	–33 29 16	0.51	0.91	6.77	11.35	30.52	10.33	
170	IRAS F12224–0624	F12224–0624	12 25 02.8	–06 40 44	< 0.11	0.20	5.99	8.13	112.70	11.27	*
171	NGC 4418	F12243–0036	12 26 54.7	–00 52 42	0.99	9.67	43.89	31.94	31.90	11.08	*
172	NGC 4433	F12250–0800	12 27 37.5	–08 16 35	0.63	1.52	13.35	23.83	41.68	10.87	
173	NGC 4575	F12351–4015	12 37 52.1	–40 32 20	0.46	0.85	7.74	16.31	58.21	10.96	
174	IC 3639	F12381–3628	12 40 51.5	–36 45 13	0.72	2.54	8.90	13.79	34.82	10.62	
175	NGC 4666	F12425–0011	12 45 07.7	–00 27 41	3.34	3.89	37.11	85.95	12.82	10.36	
176	NGC 4691	F12456–0303	12 48 13.5	–03 19 59	0.80	3.10	14.32	22.65	20.65	10.32	
177	NGC 4699	F12464–0823	12 49 02.0	–08 39 52	0.76	0.54	6.11	19.95	21.71	10.12	
178	NGC 4781	F12517–1015	12 54 24.9	–10 32 19	0.61	0.67	8.04	18.27	18.63	10.00	
179	IC 3908	F12540–0717	12 56 41.1	–07 33 46	0.42	1.20	8.47	16.65	20.28	10.07	
180	NGC 4818	F12542–0815	12 56 50.0	–08 31 38	0.96	4.40	20.12	26.60	9.37	9.75	
181	ESO 443-G017	F12550–2929	12 57 44.3	–29 45 55	0.22	0.91	5.96	8.99	35.25	10.36	
182	NGC 4835	F12552–4559	12 58 08.2	–46 15 56	1.28	1.89	17.69	40.22	23.96	10.57	
183	MCG -02-33-098/9	F12596–1529	13 02 20.5	–15 46 05	0.34	1.63	7.49	9.68	72.50	11.11	*
184	ESO 507-G070	F13001–2339	13 02 51.3	–23 55 10	0.25	0.80	13.04	15.71	96.10	11.49	*
185	NGC 4945	F13025–4912	13 05 27.6	–49 28 09	27.74	42.34	625.46	1329.70	3.92	10.48	
186	ESO 323-G077	F13036–4008	13 06 26.5	–40 24 54	0.68	1.24	5.73	10.73	58.21	10.91	
187	IRAS 13052–5711	13052–5711	13 08 18.4	–57 27 30	0.13	0.45	8.17	14.58	96.54	11.34	*
188	NGC 4984	F13063–1515	13 08 58.3	–15 31 07	0.86	1.65	11.23	17.08	17.36	10.05	
189	NGC 5010	F13097–1531	13 12 25.4	–15 47 45	0.37	1.44	10.29	21.69	94.33	11.50	
190	MCG -03-34-014	F13099–1716	13 12 35.1	–17 32 27	0.81	1.07	7.76	17.14	36.41	10.61	
191	IRAS 13120–5453	13120–5453	13 15 06.2	–55 09 24	0.44	2.98	41.11	52.33	129.36	12.26	*
192	NGC 5038	F13123–1541	13 15 02.5	–15 57 08	0.25	1.47	9.15	13.28	29.82	10.39	
193	NGC 5054	F13143–1622	13 16 59.0	–16 38 04	1.12	1.50	13.01	31.53	23.87	10.46	
194	NGC 5068	F13161–2046	13 18 52.9	–21 02 25	1.04	0.97	12.50	31.39	5.61	9.17	

Table 2 *continued*

Table 2 (*continued*)

Index	Common	<i>IRAS</i>	α	δ	$S_{12\mu\text{m}}$	$S_{25\mu\text{m}}$	$S_{60\mu\text{m}}$	$S_{100\mu\text{m}}$	D_C	$\log(L_{\text{IR}}/L_\odot)$	GOALS
<i>N</i>	Name	Name	(J2000)		(Jy)	(Jy)	(Jy)	(Jy)	(Mpc)		
(1)	(2)	(3)	(4)	(5)	(6)	(7)	(8)	(9)	(10)	(11)	(12)
195	NGC 5073	F13166–1434	13 19 18.5	–14 50 30	0.31	1.46	9.37	15.02	37.09	10.60	
196	NGC 5078	F13170–2708	13 19 50.0	–27 24 37	1.08	0.95	10.54	33.70	26.32	10.50	
197	MCG -03-34-064	F13197–1627	13 22 23.5	–16 43 34	0.94	2.97	6.20	6.20	77.33	11.24	*
198	NGC 5128	F13225–4245	13 25 27.6	–43 01 12	22.15	28.25	213.29	411.89	4.03	10.11	
199	NGC 5135	F13229–2934	13 25 43.0	–29 49 54	0.63	2.38	16.86	30.97	52.15	11.17	*
200	ESO 173-G015	13242–5713	13 27 24.4	–57 29 24	1.22	7.56	81.44	100.04	32.44	11.34	*
201	NGC 5188	F13286–3432	13 31 27.7	–34 47 36	0.86	2.83	22.58	38.26	27.25	10.72	
202	IC 4280	F13301–2356	13 32 52.8	–24 12 23	0.38	0.68	6.10	12.36	74.67	11.08	*
203	NGC 5236	F13341–2936	13 36 58.8	–29 51 46	21.46	43.57	265.84	524.09	3.60	10.10	
204	NGC 5247	F13353–1737	13 38 03.4	–17 53 04	1.51	1.48	13.65	41.83	18.77	10.32	
205	NGC 5253	F13370–3123	13 39 55.2	–31 38 21	2.50	12.07	29.84	30.08	3.15	9.05	
206	ESO 221-IG008	F13473–4801	13 50 26.9	–48 16 40	0.30	1.12	5.64	5.52	58.21	10.77	
207	ESO 221-IG010	F13478–4848	13 50 57.3	–49 03 25	0.74	1.82	12.92	22.00	58.21	11.17	*
208	NGC 5427	14008–0547	14 03 25.6	–06 01 48	1.29	1.48	10.24	25.29	38.02	10.80	
209	NGC 5483	F14072–4305	14 10 25.0	–43 19 28	0.80	0.73	6.30	17.16	20.31	10.05	
210	ESO 221-G032	F14088–4909	14 12 08.9	–49 23 24	0.58	0.71	6.82	13.83	58.21	10.93	
211	NGC 5506	F14106–0258	14 13 14.0	–03 12 24	1.29	4.17	8.42	8.87	28.07	10.49	
212	IC 4402	F14179–4604	14 21 12.6	–46 17 50	0.60	1.19	8.86	18.19	18.90	10.05	
213	NGC 5595	14214–1629	14 24 12.6	–16 43 25	0.53	0.68	9.06	18.60	36.71	10.61	
214	NGC 5597	14216–1632	14 24 26.5	–16 45 43	0.71	1.55	8.37	16.33	36.68	10.63	
215	IC 4444	F14284–4311	14 31 38.8	–43 25 08	1.40	2.33	19.13	38.07	22.47	10.53	
216	NGC 5643	F14294–4357	14 32 41.1	–44 10 30	1.97	4.68	23.48	48.60	13.86	10.24	
217	IRAS F14348–1447	F14348–1447	14 37 37.3	–15 00 20	< 0.10	0.55	6.82	7.31	330.85	12.30	*
218	NGC 5713	F14376–0004	14 40 10.9	–00 17 22	1.47	2.84	22.10	37.28	26.74	10.72	
219	IRAS F14378–3651	F14378–3651	14 40 57.8	–37 04 25	< 0.10	0.67	6.72	8.08	276.04	12.15	*
220	NGC 5719	F14383–0006	14 40 55.9	–00 19 05	0.52	1.09	8.61	17.96	27.14	10.35	
221	NGC 5728	F14396–1702	14 42 24.3	–17 15 16	0.21	1.05	8.88	15.79	38.34	10.60	
222	NGC 5734	F14423–2039	14 45 08.5	–20 52 12	0.50	0.74	7.99	24.79	59.28	11.06	*
223	ESO 386-G019	F14430–3728	14 46 09.9	–37 41 04	0.31	0.79	5.99	10.36	64.00	10.91	
224	UGCA 394	F14446–1714	14 47 24.1	–17 26 49	0.30	1.04	5.83	10.61	30.02	10.26	
225	NGC 5757	F14449–1852	14 47 46.3	–19 04 43	0.77	0.94	6.57	12.56	36.29	10.53	
226	IC 4518A/B	F14544–4255	14 57 43.1	–43 08 01	0.36	1.53	8.07	13.65	69.94	11.13	*
227	NGC 5786	F14556–4148	14 58 56.9	–42 00 51	0.37	0.98	5.90	15.00	35.04	10.45	
228	NGC 5792	F14558–0053	14 58 22.9	–01 05 26	0.97	1.00	9.08	20.32	25.36	10.36	
229	NGC 5793	F14565–1629	14 59 23.5	–16 41 28	0.17	0.49	6.48	9.44	50.17	10.65	
230	NGC 5861	F15065–1107	15 09 15.4	–11 19 16	0.72	1.54	11.41	20.53	23.84	10.34	
231	NGC 5833	F15066–7240	15 11 51.0	–72 51 28	0.83	0.99	7.29	22.42	38.65	10.69	
232	UGCA 402	F15106–2029	15 13 30.6	–20 40 29	0.54	0.64	5.70	14.37	30.94	10.34	
233	NGC 5915	F15188–1254	15 21 33.7	–13 05 34	0.46	1.36	10.71	16.41	32.94	10.55	

Table 2 *continued*

Table 2 (*continued*)

Index	Common	<i>IRAS</i>	α	δ	$S_{12\mu\text{m}}$	$S_{25\mu\text{m}}$	$S_{60\mu\text{m}}$	$S_{100\mu\text{m}}$	D_C	$\log(L_{\text{IR}}/L_\odot)$	GOALS
<i>N</i>	Name	Name	(J2000)		(Jy)	(Jy)	(Jy)	(Jy)	(Mpc)	(11)	(12)
(1)	(2)	(3)	(4)	(5)	(6)	(7)	(8)	(9)	(10)		
234	ESO 099-G004	15206–6256	15 24 57.1	–63 07 29	0.29	1.46	10.30	13.65	123.07	11.67	*
235	NGC 5937	F15281–0239	15 30 46.0	–02 49 45	0.68	1.47	10.41	21.47	42.45	10.83	
236	NGC 6000	F15467–2914	15 49 49.4	–29 23 11	1.48	5.35	35.64	54.94	28.90	10.97	
237	ESO 137-G014	16129–5811	16 17 10.0	–58 18 43	0.29	1.00	6.16	8.12	34.99	10.37	
238	IC 4595	F16154–7001	16 20 44.4	–70 08 35	0.70	0.67	7.05	18.64	45.75	10.78	
239	IRAS F16164–0746	F16164–0746	16 19 10.3	–07 53 57	0.17	0.59	10.29	13.22	115.46	11.55	*
240	ESO 452-G005	16285–2759	16 31 40.2	–28 06 11	1.03	1.18	6.44	...	61.25	10.90	
241	NGC 6156	16304–6030	16 34 51.9	–60 37 08	1.23	2.71	17.17	32.00	43.96	11.07	*
242	ESO 069-IG006	F16330–6820	16 38 11.4	–68 26 07	0.25	0.71	7.08	12.68	188.61	11.92	*
243	IRAS F16399–0937	F16399–0937	16 42 39.2	–09 43 11	0.27	1.13	8.42	14.72	114.61	11.56	*
244	ESO 453-G005	F16443–2915	16 47 29.8	–29 21 17	< 0.11	0.61	9.56	12.17	91.55	11.29	*
245	NGC 6215	16467–5854	16 51 06.7	–58 59 38	1.94	3.53	29.97	47.55	19.04	10.54	
246	NGC 6221	16484–5908	16 52 46.1	–59 13 00	3.11	7.48	49.07	86.06	18.02	10.73	
247	IRAS F16516–0948	F16516–0948	16 54 24.2	–09 53 22	0.27	0.49	5.32	11.65	96.87	11.24	*
248	NGC 6300	F17123–6245	17 17 00.3	–62 49 13	1.71	3.25	16.72	42.45	13.11	10.09	
249	IRAS F17138–1017	F17138–1017	17 16 36.3	–10 20 40	0.63	2.12	15.18	19.02	75.84	11.42	*
250	IRAS F17207–0014	F17207–0014	17 23 21.4	–00 17 00	0.20	1.61	32.13	36.08	175.68	12.39	*
251	ESO 138-G027	F17222–5953	17 26 43.7	–59 55 56	0.33	1.35	9.53	11.05	88.80	11.34	*
252	IC 4662	F17422–6437	17 47 06.9	–64 38 17	0.27	1.27	8.82	11.38	1.69	7.85	
253	IRAS 17578–0400	17578–0400	18 00 32.0	–04 00 55	0.22	1.14	27.69	33.10	58.62	11.35	*
254	IC 4687/6	F18093–5744	18 13 38.6	–57 43 36	1.01	3.55	20.20	27.54	74.12	11.55	*
255	ESO 140-G012	F18097–6006	18 14 17.4	–60 05 30	0.41	1.02	5.69	9.51	43.60	10.58	
256	IRAS F18293–3413	F18293–3413	18 32 40.2	–34 11 26	1.14	3.98	35.71	53.38	77.76	11.81	*
257	IC 4734	F18341–5732	18 38 26.5	–57 29 24	0.38	1.33	14.04	25.31	68.57	11.30	*
258	NGC 6744	NGC 6744	19 09 45.9	–63 51 27	2.97	3.46	18.92	70.21	9.90	9.99	
259	NGC 6753	F19071–5707	19 11 22.5	–57 02 59	0.94	0.98	9.79	27.14	43.93	10.89	
260	ESO 593-IG008	F19115–2124	19 14 30.7	–21 19 08	0.18	0.51	6.38	9.37	196.19	11.87	*
261	IRAS F19297–0406	F19297–0406	19 32 22.1	–04 00 02	< 0.10	0.69	7.32	8.62	338.24	12.37	*
262	NGC 6808	F19384–7045	19 43 53.9	–70 37 58	0.75	0.87	7.36	17.91	47.85	10.83	
263	NGC 6810	F19393–5846	19 43 33.6	–58 39 22	1.27	3.55	18.20	32.60	27.37	10.69	
264	NGC 6814	F19398–1026	19 42 38.4	–10 19 28	0.92	1.04	6.53	19.67	24.04	10.25	
265	NGC 6822	NGC 6822	19 44 56.8	–14 48 24	0.25	2.46	47.63	95.42	0.54	7.58	
266	NGC 6835	F19517–1241	19 54 33.5	–12 34 02	0.65	1.37	11.16	16.82	24.55	10.32	
267	ESO 339-G011	F19542–3804	19 57 37.5	–37 56 10	0.36	1.20	5.96	9.27	79.84	11.12	*
268	IC 4946	F20205–4409	20 23 56.8	–43 59 46	0.26	0.65	5.24	6.74	41.26	10.42	
269	NGC 6907	F20221–2458	20 25 05.9	–24 48 32	1.19	1.94	14.14	29.59	45.08	11.03	*
270	NGC 6918	F20272–4738	20 30 47.7	–47 28 23	0.30	1.34	9.17	13.76	24.95	10.23	
271	NGC 6926	F20304–0211	20 33 04.8	–02 01 39	0.63	1.03	7.09	14.38	81.94	11.26	*
272	IC 5063	F20482–5715	20 52 03.5	–57 04 03	1.11	3.94	5.87	4.25	47.19	10.85	

Table 2 *continued*

Table 2 (*continued*)

Index	Common Name	<i>IRAS</i>	α	δ	$S_{12\mu\text{m}}$	$S_{25\mu\text{m}}$	$S_{60\mu\text{m}}$	$S_{100\mu\text{m}}$	D_{C}	$\log(L_{\text{IR}}/L_{\odot})$	GOALS
<i>N</i>	Name	Name	(J2000)		(Jy)	(Jy)	(Jy)	(Jy)	(Mpc)		
(1)	(2)	(3)	(4)	(5)	(6)	(7)	(8)	(9)	(10)	(11)	(12)
273	ESO 286-IG019	F20551-4250	20 58 27.4	-42 38 57	0.28	1.87	12.19	10.31	172.76	12.00	*
274	ESO 286-G035	F21008-4347	21 04 11.2	-43 35 34	0.42	0.81	8.55	12.60	71.98	11.13	*
275	ESO 402-G026	F21194-3653	21 22 33.5	-36 40 44	0.33	0.77	6.59	12.00	37.98	10.49	
276	NGC 7083	F21318-6407	21 35 43.9	-63 54 08	0.71	0.87	5.84	16.40	32.84	10.45	
277	NGC 7090	F21329-5446	21 36 28.4	-54 33 30	0.43	0.76	8.15	19.74	7.65	9.22	
278	ESO 343-IG013	F21330-3846	21 36 10.8	-38 32 38	0.28	0.87	6.27	8.69	77.99	11.07	*
279	NGC 7130	F21453-3511	21 48 19.6	-34 57 05	0.58	2.16	16.71	25.89	65.99	11.35	*
280	NGC 7172	F21591-3206	22 02 02.2	-31 52 09	0.42	0.88	5.76	12.42	36.16	10.45	
281	NGC 7205	F22051-5741	22 08 34.4	-57 26 35	1.00	1.51	9.80	27.72	16.66	10.07	
282	ESO 467-G027	F22118-2742	22 14 40.2	-27 27 49	0.44	0.58	5.58	12.48	70.88	11.02	*
283	IC 5179	F22132-3705	22 16 10.0	-36 50 35	1.18	2.40	19.39	37.29	46.70	11.16	*
284	ESO 602-G025	F22287-1917	22 31 27.4	-19 01 55	0.27	0.91	5.42	9.64	99.73	11.27	*
285	ESO 534-G009	F22359-2606	22 38 40.8	-25 51 05	0.46	0.63	6.03	11.78	46.16	10.65	
286	ESO 239-IG002	F22467-4906	22 49 39.6	-48 51 01	0.10	1.17	7.24	7.92	170.03	11.78	*
287	IRAS F22491-1808	F22491-1808	22 51 49.0	-17 52 27	< 0.09	0.54	5.54	4.64	301.83	12.11	*
288	NGC 7418	F22537-3717	22 56 35.4	-37 01 54	0.66	0.69	6.67	16.07	19.79	10.01	
289	NGC 7496	F23069-4341	23 09 46.1	-43 25 43	0.58	1.93	10.14	16.57	22.34	10.23	
290	ESO 148-IG002	F23128-5919	23 15 46.6	-59 03 14	0.35	1.64	10.94	10.68	177.75	12.00	*
291	NGC 7552	F23133-4251	23 16 09.5	-42 35 09	3.76	11.92	77.37	102.92	21.44	11.03	*
292	NGC 7582	F23156-4238	23 18 22.2	-42 22 19	2.30	7.39	52.20	82.86	21.29	10.87	
293	NGC 7592	F23157-0441	23 18 22.2	-04 24 56	0.26	0.97	8.05	10.58	95.13	11.33	*
294	NGC 7590	F23161-4230	23 18 55.5	-42 14 17	0.69	0.89	7.69	20.79	21.58	10.16	
295	NGC 7599	F23165-4231	23 19 20.6	-42 15 25	0.74	0.77	6.39	18.31	22.38	10.14	
296	ESO 077-IG014	F23180-6929	23 21 05.0	-69 12 49	0.20	0.45	5.70	9.90	166.27	11.70	*
297	MCG -01-60-022	F23394-0353	23 42 02.2	-03 36 48	0.41	1.06	5.39	8.26	91.19	11.21	*
298	NGC 7793	F23552-3252	23 57 48.5	-32 35 28	1.32	1.67	18.14	54.07	3.10	8.84	

NOTE—Table 2 is published in its entirety in the machine-readable format.

The multipanel fig. 1 in Sanders et al. (2003) presents an atlas of Digitized Sky Survey (DSS1) optical images for all RBGS sources with elliptical overlays bounding the *IRAS* 3σ position uncertainties.

3.2. The 1.28 GHz MeerKAT image atlas

The cropped 1.28 GHz Stokes I images are displayed individually as gray-scale images in Figure Set 2 with labels indicating their source index numbers in Table 2; e.g., the $N = 298$ source identified with NGC 7793 appears in Figure 2.298. These images are also available in FITS format from <https://doi.org/10.48479/dnt7-6q05>

Fig. Set 2. 1.28 GHz MeerKAT images of southern sources in the *IRAS* RBGS.

The full Figure Set 2 is available in .pdf format from <ftp://ftp.cv.nrao.edu/NRAO-staff/jcondon/RBGS.dir/MeerKAT.dir/pdf.dir/>.

Figure 3 compares $3' \times 3'$ MeerKAT 1.28 GHz and *Herschel* $\lambda = 100\mu\text{m}$ image cutouts centered on NGC 6156. When observed at the same resolution, most RBGS galaxies have similar radio and FIR morphologies. The faint radio source to the right of NGC 6156 is a background source with no detectable FIR counterpart, and confusing background AGNs are more common at radio wavelengths.

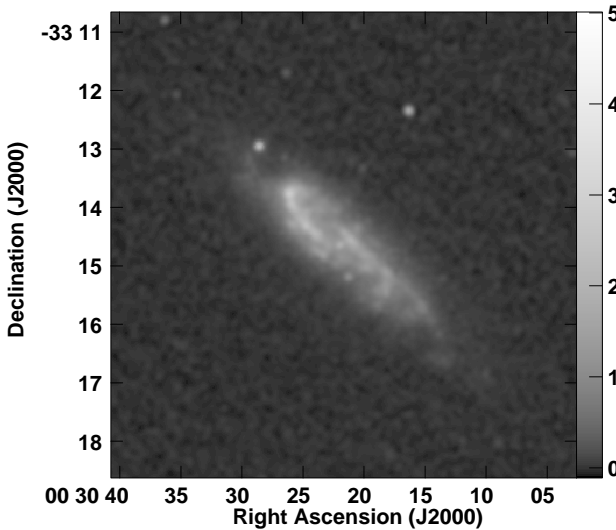


Figure 2. This MeerKAT 1.28 GHz image of NGC 0134 is displayed over the intensity range $-0.1 < S_p(\text{mJy beam}^{-1}) < 5$ indicated by the scale bar in units of mJy beam^{-1} on the right. The complete figure set of 298 MeerKAT images is available.

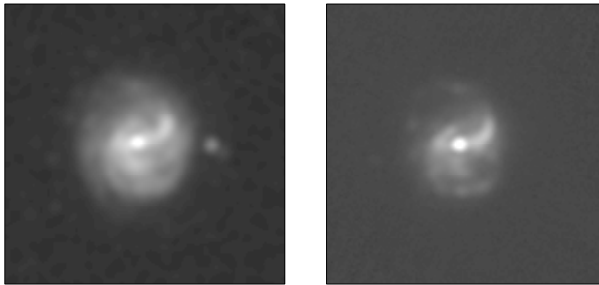


Figure 3. Comparison of $3' \times 3'$ images of NGC 6156 from MeerKAT (left) at $\nu = 1.28 \text{ GHz}$ and $7.4''$ resolution and from *Herschel* (right) at $\lambda = 100 \mu\text{m}$ and $6.8''$ resolution (Chu et al. 2017).

3.3. Basic 1.28 GHz MeerKAT source parameters

We extracted basic parameters describing the 1.28 GHz radio sources identified with RBGS sources or individual galaxies in our MeerKAT images. The total 1.28 GHz flux density S from each *IRAS* source was obtained in an aperture covering all of its radio emission by summing over pixel brightnesses using the *AIPS* verb *TVSTAT*. The *AIPS* verb *MAXFIT* was used to estimate the peak flux densities S_p and equinox J2000 equatorial coordinates of compact components embedded in bright extended emission. Otherwise, the *AIPS* task *JMFIT* was used to make Gaussian fits to component peak flux densities S_p , integrated flux densities S_I ,

deconvolved size parameters (FWHM major axis ϕ_M , minor axis ϕ_m , and position angle *PA* measured counterclockwise from north), and equinox J2000 equatorial coordinates. Some of these compact components are surrounded by faint extended disk emission, which the Gaussian fits ignored by excluding pixels fainter than 10% of the peak brightness. In most RBGS sources the disk emission is much more extended than the fitted core component. The detailed brightness distributions of components smaller than the beam are indeterminate, and any deconvolved component FWHM $\phi_M \lesssim 7.5''$ implies only that the second moment of the component brightness distribution equals that of a Gaussian with FWHM = ϕ_M .

We compared our 1.28 GHz flux densities with the 1.4 GHz flux densities of NVSS (Condon et al. 1998) sources north of the NVSS declination limit $\delta > -40^\circ$ because only the NVSS images have the surface-brightness sensitivity ($\sigma = 0.45 \text{ mJy beam}^{-1}$ in a $\theta_M = \theta_m = 45''$ beam, which corresponds to $T_b = 0.14 \text{ K}$) needed to detect almost all RBGS sources. Most RBGS sources are dominated by optically thin synchrotron radiation and have spectral indices $\alpha \approx -0.7$, so we expect them to lie near the line $\langle S(1.4 \text{ GHz})/S(1.28 \text{ GHz}) \rangle \approx 0.94$ in Figure 4.

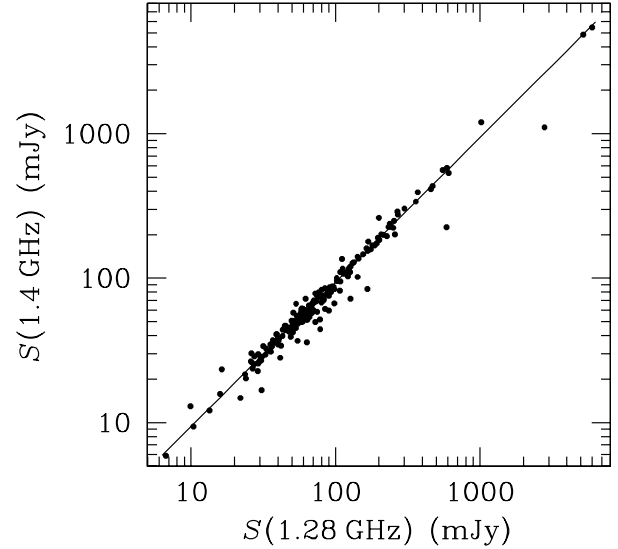


Figure 4. The MeerKAT 1.28 GHz flux densities and NVSS 1.4 GHz flux densities of RBGS galaxies north of $\delta = -40^\circ$ cluster around the line $S(1.4 \text{ GHz})/S(1.28 \text{ GHz}) = 0.936$ expected for sources with spectral index $\alpha = -0.74$.

The 1.4 GHz flux densities of some NVSS sources fall significantly below that line, usually because the NVSS catalog is incomplete for emission fainter than

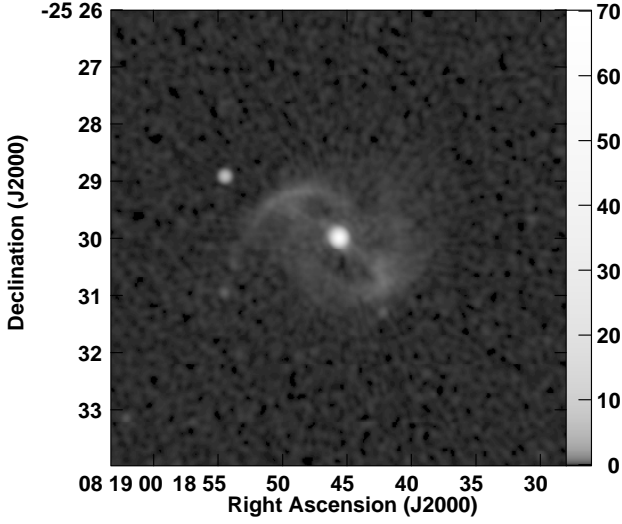


Figure 5. The diffuse emission surrounding the center of NGC 2566 visible in our 1.28 GHz MeerKAT image is too faint to contribute to the NVSS cataloged flux density. The scale bar on the right indicates intensity in mJy beam^{-1} .

$S_p = 2.4 \text{ mJy beam}^{-1}$. For example, the $S(1.4 \text{ GHz}) = 102 \text{ mJy}$ NVSS flux density of NGC 2566 does not include the faint disk surrounding the compact nuclear component (Figure 5), which is included in the MeerKAT flux density $S(1.28 \text{ GHz}) = 142 \text{ mJy}$.

The distribution of the logarithmic flux-density ratio $\log[S(1.4 \text{ GHz})/S(1.28 \text{ GHz})]$ shown by the histogram in Figure 6 has a narrow (semi-interquartile range 0.0235) peak indicating good linearity and rms intensity-proportional errors $\lesssim 5\%$ at each frequency. The median of the distribution is $\langle \log[S(1.4 \text{ GHz})/S(1.28 \text{ GHz})] \rangle = -0.0287$, which corresponds to perfect MeerKAT/NVSS flux-density scale agreement for sources with median spectral index $\langle \alpha(1.28 \text{ GHz}/1.4 \text{ GHz}) \rangle = -0.74$. Conversely, if the actual median spectral index is anywhere in the range $-0.84 < \langle \alpha \rangle < -0.64$, the 1.28 GHz MeerKAT and 1.4 GHz NVSS flux-density scales must agree within 1%, which is even better than expected.

The VLA has imaged most RBGS galaxies north of $\delta = -45^\circ$ at $\nu = 1.49 \text{ GHz}$ at one or more resolutions between $\theta_M \approx 2''$ and $\theta_M = 60''$ with rms noise in the range $0.1 < \sigma_n(\text{mJy beam}^{-1}) < 0.2$ (Condon et al. 1990, 1996). The flux-density agreement is good for most of the compact radio sources, but the limited surface-brightness sensitivity often caused the VLA to miss extended emission and yield flux densities significantly lower than the MeerKAT flux densities. Comparison of deconvolved angular sizes measured in VLA images having $\theta_M \approx 2''$ resolution confirms that the

MeerKAT deconvolved angular-size estimates of sources as small as $\phi_M \sim 2''$ are reliable.

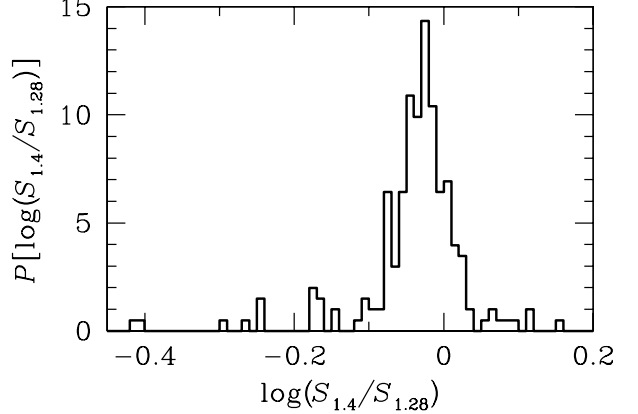


Figure 6. Histogram of the logarithmic flux-density ratio $\log[(S(1.4 \text{ GHz})/S(1.28 \text{ GHz})]$. The narrow peak indicates small intensity-proportional errors and the median $\langle \log[S(1.4 \text{ GHz})/S(1.28 \text{ GHz})] \rangle = -0.0287$ is expected for sources with spectral index $\alpha = -0.74$.

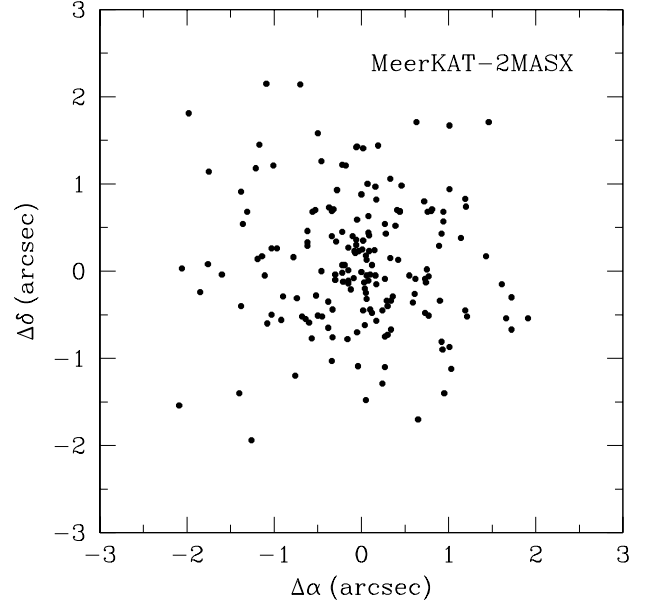


Figure 7. For galaxies with well-defined nuclei, this scatter plot shows the distribution of MeerKAT minus 2MASX offsets in right ascension $\Delta\alpha$ and declination $\Delta\delta$.

We estimated the absolute astrometric uncertainties in our MeerKAT 1.28 GHz image by comparing fitted

positions of strong compact sources in those images with very accurate positions in the third realization of the International Celestial Reference Frame (Charlot et al. 2020). The rms uncertainties in right ascension and declination are $\sigma_\alpha \approx 0''.5$ and $\sigma_\delta \approx 0''.6$, respectively. This is larger than the $0''.1$ we hoped for. Possible causes include (1) large angular separations between targets and calibration sources, (2) no on-line interferometric refraction correction, and (3) no UT1 corrections in the on-line delay model.

More relevant for most astronomical applications are the relative uncertainties of our 1.28 GHz component positions compared with their infrared positions. For components smaller than the MeerKAT synthesized beam ($\phi_M \lesssim 7''.5$) in galaxies with well-defined nuclei, the distribution of MeerKAT minus accurate ($\sigma_\alpha \approx \sigma_\delta \approx 0''.1$) 2MASX coadded positions (Skrutskie et al. 2006) is shown in Figure 7. The rms scatters in the offsets are $\sigma_{\Delta\alpha} = 1''.0$ and $\sigma_{\Delta\delta} = 1''.1$. The mean offsets in right ascension and declination are $\langle \Delta\alpha \rangle = -0''.09 \pm 0''.07$ and $\langle \Delta\delta \rangle + 0''.05 \pm 0''.08$, both consistent with zero.

Table 3 presents the 1.28 GHz MeerKAT source parameters of the southern RBGS sample:

Column (1).—Our *IRAS* source index number N from Table 2 running from 1 through 298.

Column (2).—The most common galaxy name(s). If an *IRAS* source contains multiple galaxies resolved by

MeerKAT, the individual galaxies are listed in additional rows with the same index number N .

Column (3).—Total 1.28 GHz MeerKAT flux density S (mJy) associated with the *IRAS* source.

Columns (4)-(10).—The 1.28 GHz component parameters determined by fitting only the component peak or by a full Gaussian fit.

Column (4).—Component peak flux density in mJy per Gaussian beam solid angle $\Omega_b = \pi\theta_M\theta_m/(4\ln 2)$.

Column (5).—Component integrated flux density (mJy) from a Gaussian fit.

Columns (6)-(8).—Gaussian fit deconvolved component FWHM major axis, minor axis, and major axis position angle measured counterclockwise from north.

Columns (9)-(10).—Component J2000 right ascension α and declination δ . Positions listed with $0''.01$ precision in α and $0''.1$ in δ have rms uncertainties $\sigma_\alpha = \sigma_\delta = 1''$. Galaxies lacking clearly defined radio nuclei have positions listed with $0''.1$ precision in α and $1''$ in δ and have rms uncertainties between $1''$ and $10''$ in each coordinate.

Columns (11)-(13).—The image restoring beam FWHM major axis θ_M , minor axis θ_m , and major-axis position angle BPA measured counterclockwise from north.

Column (14).—Observing run label from Table 1.

Table 3. The Southern RBGS Sample: 1.28 GHz MeerKAT Data

Index N (1)	Common Name (2)	S (mJy) (3)	S_P (mJy/ Ω_b) (4)	S_I (mJy) (5)	ϕ_M ($''$) (6)	ϕ_m ($''$) (7)	PA ($^{\circ}$) (8)	α (J2000) (9)	δ ($''$) (10)	θ_M ($''$) (11)	θ_m ($''$) (12)	BPA ($^{\circ}$) (13)	Run (14)
001 NGC 0034		98.0	58.5	61.6	1.9	1.7	4	00 11 06.57	-12 06 27.2	7.68	7.67	-1	H
002 NGC 0055		587.	7.74	16.3	8.3	7.4	-79	00 14 57.54	-39 12 25.8	7.48	7.22	89	K
003 MCG -02-01-051/2		45.2								7.68	7.67	-1	H
003 MCG -02-01-051			30.7	40.0	4.8	3.6	-54	00 18 50.88	-10 22 36.6	7.68	7.67	-1	H
003 MCG -02-01-052				2.8				00 18 49.99	-10 21 29.9	7.68	7.67	-1	H
004 NGC 0134		227.	1.8					00 30 21.96	-33 14 38.0	7.57	7.37	-28	K
005 ESO 079-G003		61.7	14.8	23.5	7.9	3.2	-50	00 32 02.36	-64 15 10.9	7.61	7.34	-1	C
006 NGC 0150		58.2	17.4	21.0	3.6	3.0	80	00 34 15.46	-27 48 12.5	7.59	7.25	0	H
007 NGC 0157		193.						00 34 46.5	-08 23 50.	7.68	7.67	81	H
008 ESO 350-IG038		30.5	25.0	29.5	3.5	2.8	86	00 36 52.56	-33 33 16.4	7.65	7.37	-88	C
009 NGC 0174		47.4	30.9	43.4	6.4	2.9	-37	00 36 58.92	-29 28 39.9	7.67	7.18	-14	H
010 NGC 0232		64.9	50.4	60.9	3.5	3.3	82	00 42 45.81	-23 33 40.9	7.72	7.18	-6	H
011 NGC 0247		20.0						00 47 07.2	-20 45 50.	7.55	7.50	-44	H

Table 3 *continued*

Table 3 (*continued*)

Index <i>N</i> (1)	Common Name (2)	<i>S</i> (mJy) (3)	<i>S_P</i> (mJy/ Ω_b) (4)	<i>S_I</i> (mJy) (5)	ϕ_M ($''$) (6)	ϕ_m ($''$) (7)	<i>PA</i> ($^{\circ}$) (8)	α (J2000) (9)	δ ($''$) (10)	θ_M ($''$) (11)	θ_m ($''$) (12)	<i>BPA</i> ($^{\circ}$) (13)	Run (14)
012	NGC 0253	5970.	1080.	2130.	10.2	4.5	55	00 47 33.14 -25 17 17.9	7.54	7.44	-34	H	
013	NGC 0289	51.7	2.2	4.3	9.4	4.8	-37	00 52 42.41 -31 12 21.0	7.47	7.37	90	C	
014	NGC 0300	104.						00 54 56.2 -37 40 41.	7.63	7.34	84	C	
015	NGC 0337	114.	5.2					00 59 50.7 -07 34 58.	7.57	7.55	88	H	
016	IC 1623A/B	255.							7.58	7.41	-30	H	
016	IC 1623A		46.0	97.8	8.1	7.7	21	01 07 46.74 -17 30 25.0	7.58	7.41	-30	H	
016	IC 1623B		69.8	144.4	7.8	7.6	60	01 07 47.44 -17 30 25.1	7.58	7.41	-30	H	
017	MCG -03-04-014	48.1	33.3	45.9	5.4	3.8	-44	01 10 08.95 -16 51 09.9	7.68	7.52	14	H	
018	ESO 244-G012	62.5							7.64	7.27	-74	C	
018	ESO 244-G012 NED01		2.4	7.3	12.9	8.8	-32	01 18 08.26 -44 27 58.9	7.64	7.27	-74	C	
018	ESO 244-G012 NED02		48.8	54.1	2.6	2.4	-56	01 18 08.41 -44 27 42.2	7.64	7.27	-74	C	
019	NGC 0613	251.	59.6	98.7	6.7	5.4	-73	01 34 18.21 -29 25 07.0	7.51	7.37	0	H	
020	ESO 353-G020	104.	76.0	97.8	4.7	3.2	89	01 34 51.37 -36 08 13.4	7.45	7.36	87	C	
021	NGC 0625	12.1	5.5					01 35 06.99 -41 26 12.6	7.66	7.19	-27	K	
022	ESO 297-G011/012	50.0							7.40	7.39	89	C	
022	ESO 297-G011	36.3	11.1	27.1	10.0	7.8	-35	01 36 23.49 -37 19 17.4	7.40	7.39	89	C	
022	ESO 297-G012		12.1	12.7	2.0	1.3	-49	01 36 24.24 -37 20 25.3	7.40	7.39	89	C	
023	IRAS F01364-1042	15.9	15.4	15.7	< 1.2			01 38 52.88 -10 27 11.7	7.56	7.53	89	H	
024	NGC 0643B	46.7	20.1	42.7	12.2	4.2	-71	01 39 12.92 -75 00 39.5	8.26	7.44	54	C	
025	NGC 0701	50.7	3.4	38.4	35.6	16.6	49	01 51 03.77 -09 42 10.1	7.92	7.37	51	H	
026	NGC 0835	50.4	17.9	41.9	10.0	7.7	6	02 09 24.60 -10 08 09.5	7.68	7.56	47	H	
027	NGC 0838	97.0	43.2	90.2	9.9	6.0	-89	02 09 38.56 -10 08 47.2	7.68	7.56	47	H	
028	NGC 0839	41.9	37.2	40.8	2.9	1.8	81	02 09 42.76 -10 11 02.2	7.68	7.56	47	H	
029	NGC 0873	60.3	12.8					02 16 32.39 -11 20 54.1	7.55	7.50	36	H	
030	NGC 0908	207.	5.5					02 23 04.59 -21 14 02.2	7.50	7.46	56	H	
031	NGC 0922	59.8	3.6					02 25 04.51 -24 47 16.6	7.60	7.36	-24	M	
032	NGC 0958	70.8	2.5					02 30 43.0 -02 56 20.	7.65	7.60	85	C	
033	NGC 0986	126.	38.8	66.8	8.1	4.6	-70	02 33 34.31 -39 02 41.9	7.67	7.27	90	K	
034	NGC 1022	44.5	30.9	40.5	4.8	3.6	-16	02 38 32.72 -06 40 38.1	7.63	7.41	-2	M	
035	NGC 1068	5200.	2800.	4300.	8.2	2.2	38	02 42 40.85 -00 00 46.3	7.63	7.60	8	C	
036	NGC 1083	58.0	16.1	43.1	14.0	5.8	21	02 45 40.65 -15 21 27.7	7.77	7.10	-1	M	
037	NGC 1084	269.	6.7					02 45 59.89 -07 34 42.4	7.59	7.49	-33	M	
038	NGC 1087	111.	4.1	33.7	25.	17.	-71	02 46 25.26 -00 29 56.3	7.64	7.55	-16	M	
039	NGC 1097	457.	24.4	269.	25.	23.	-82	02 46 18.92 -30 16 30.0	7.62	7.35	-7	M	
040	NGC 1187	70.6	15.9	20.7	4.5	3.6	-74	03 02 37.59 -22 52 01.6	7.66	7.24	-9	M	
041	NGC 1204	26.4	23.9	25.5	2.3	1.6	64	03 04 39.94 -12 20 28.9	9.02	6.86	-31	M	
042	NGC 1222	58.5	24.6	51.4	10.2	5.5	89	03 08 56.80 -02 57 18.3	7.60	7.48	-22	M	
043	NGC 1232	89.9						03 09 46.4 -20 34 51.	7.65	7.24	-19	M	
044	NGC 1266	112.	88.7	111.	5.0	2.2	-6	03 16 00.76 -02 25 39.1	7.62	7.54	-30	M	

Table 3 *continued*

Table 3 (*continued*)

Index <i>N</i> (1)	Common Name (2)	<i>S</i> (mJy) (3)	<i>S_P</i> (mJy/ Ω_b) (4)	<i>S_I</i> (mJy) (5)	ϕ_M ($''$) (6)	ϕ_m ($''$) (7)	<i>PA</i> ($^{\circ}$) (8)	α (J2000) (9)	δ ($''$) (10)	θ_M ($''$) (11)	θ_m ($''$) (12)	<i>BPA</i> ($^{\circ}$) (13)	Run (14)
045	NGC 1313	336.						03 18 12.5	-66 30 27.	7.68	7.34	-84	C
046	NGC 1309	62.1	1.1					03 22 06.0	-15 23 52.	7.74	7.16	-7	M
047	NGC 1326	33.1	8.8	31.9	14.5	9.7	76	03 23 56.49	-36 27 53.6	7.43	7.39	0	K
048	IC 1953	9.9	2.1	2.2	< 2.1			03 33 41.85	-21 28 43.9	7.57	7.35	-25	M
049	NGC 1365	607.	75.3	401.	21.7	10.5	29	03 33 36.48	-36 08 24.3	7.62	7.30	-85	C
050	NGC 1377	0.42	0.32	0.42	6.	< 2.	13	03 36 39.04	-20 54 08.5	7.68	7.37	-14	M
051	NGC 1386	36.8	25.0	29.4	4.0	2.1	-30	03 36 46.19	-35 59 58.3	7.93	7.19	-67	K
052	NGC 1385	169.	5.2					03 37 28.7	-24 30 03.	7.46	7.39	3	M
053	NGC 1406	142.	9.4	63.4	18.9	11.6	18	03 39 23.16	-31 19 19.3	7.48	7.42	-6	K
054	NGC 1415	27.2	6.0	25.3	20.0	8.3	-23	03 40 56.86	-22 33 54.0	7.67	7.39	-88	M
055	NGC 1421	108.	6.0	22.8	15.2	10.2	10	03 42 29.30	-13 29 17.0	7.52	7.51	14	M
056	NGC 1448	121.	2.7					03 44 31.75	-44 38 41.3	7.64	7.29	-77	K
057	NGC 1482	238.	94.6	203.	10.4	5.6	-73	03 54 38.97	-20 30 08.4	7.54	7.44	-25	M
058	NGC 1511	180.	9.5					03 59 36.3	-67 38 01.	7.77	7.35	-70	C
059	NGC 1532	122.	1.2					04 12 04.31	-32 52 27.2	7.60	7.34	88	K
060	ESO 420-G013	65.4	53.4	63.5	2.9	2.4	58	04 13 49.73	-32 00 25.2	7.71	7.22	-64	C
061	NGC 1546	36.5						04 14 36.3	-56 03 41.	7.84	7.22	-71	C
062	IC 2056	35.7	2.3	30.5	28.	25.	59	04 16 24.43	-60 12 23.8	7.87	7.11	-55	C
063	NGC 1559	347.	3.3					04 17 36.4	-62 47 01.	7.77	7.27	-72	C
064	NGC 1566	286.	31.4	33.6	2.5	1.3	-71	04 20 00.35	-54 56 16.7	7.83	7.08	-57	C
065	ESO 550-IG025	39.3								7.66	7.27	-16	M
065	ESO 550-IG025 NED01	24.0	15.5	21.6	5.3	4.0	2	04 21 19.99	-18 48 39.9	7.66	7.27	-16	M
065	ESO 550-IG025 NED02	15.3	12.7	14.5	2.8	1.9	10	04 21 20.04	-18 48 57.7	7.66	7.27	-16	M
066	NGC 1572	52.6	39.2	45.8	3.8	2.2	-5	04 22 42.82	-40 36 03.1	7.75	7.20	-70	C
067	NGC 1614	144.	102.	124.	3.9	3.1	71	04 34 00.05	-08 34 45.6	7.61	7.60	-63	M
068	ESO 485-G003	51.1	17.2	43.9	11.4	7.3	-12	04 39 06.39	-24 11 03.3	7.63	7.24	-13	M
069	NGC 1637	22.0	5.5	7.0	4.2	3.6	8	04 41 28.27	-02 51 29.2	7.62	7.53	-32	M
070	NGC 1672	341.	31.5	150.	16.9	12.7	-43	04 45 42.41	-59 14 50.0	7.85	7.32	-77	C
071	ESO 203-IG001	10.8	10.6	10.6	< 1.			04 46 49.52	-48 33 30.3	7.83	7.12	-58	C
072	NGC 1667	74.3	6.4					04 48 37.18	-06 19 11.7	7.76	7.49	-40	I
073	MCG -05-12-00	24.0	22.2	23.5	2.0	1.4	41	04 52 05.03	-32 59 25.2	7.64	7.23	22	E
074	IC 0398	29.1	25.0	27.3	2.7	1.8	30	04 58 12.54	-07 46 49.2	7.68	7.51	-44	I
075	NGC 1720	45.0	29.5	34.9	3.7	2.8	84	04 59 20.62	-07 51 32.0	7.77	7.46	-50	I
076	NGC 1792	300.	4.6					05 05 14.39	-37 58 51.9	7.89	7.35	-78	K
077	NGC 1797	30.9	20.5	26.0	4.2	3.6	56	05 07 44.93	-08 01 08.0	7.65	7.60	26	E
078	NGC 1808	553.	130.	419.	14.0	8.8	-40	05 07 42.41	-37 30 47.4	7.85	7.28	-76	I
079	NGC 1832	59.4	2.9	5.7	8.1	6.9	7	05 12 03.37	-15 41 15.6	7.72	7.36	-46	I
080	IRAS F05187-1017	26.2	25.4	26.1	1.5	1.1	-71	05 21 06.55	-10 14 45.7	7.66	7.43	-47	I
081	IRAS F05189-2524	27.5	26.7	27.3	1.1	< 1.		05 21 01.40	-25 21 45.1	7.79	7.42	24	I

Table 3 *continued*

Table 3 (*continued*)

Index	Common Name	<i>S</i>	<i>S_P</i>	<i>S_I</i>	ϕ_M	ϕ_m	<i>PA</i>	α	δ	θ_M	θ_m	<i>BPA</i>	
<i>N</i>	Name	(mJy)	(mJy/ Ω_b)	(mJy)	($''$)	($''$)	($^{\circ}$)	(J2000)		($''$)	($''$)	($^{\circ}$)	Run
(1)	(2)	(3)	(4)	(5)	(6)	(7)	(8)	(9)	(10)	(11)	(12)	(13)	(14)
082	NGC 1964	63.4						05 33 21.6	-21 56 44.	7.68	7.34	-44	I
083	NGC 2076	58.0						05 46 47.4	-16 47 00.	7.63	7.48	-44	I
084	NGC 2139	72.6	2.1					06 01 07.8	-23 40 20.	7.61	7.34	-48	I
085	ESO 121-G006	106.	69.7	73.8	2.3	1.3	39	06 07 29.67	-61 48 26.6	7.73	7.21	38	E
086	IRAS F06076-2139	23.6	19.8	21.1	2.4	1.2	-21	06 09 45.81	-21 40 23.4	8.01	7.28	49	E
087	NGC 2207/IC 2163	371.	1.2							7.63	7.46	-44	I
087	NGC 2207		1.2					06 16 22.02	-21 22 22.3	7.63	7.46	-44	I
087	IC 2163		1.9					06 16 27.3	-21 22 28.	7.63	7.46	-44	I
088	UGCA 127	201.						06 20 56.7	-08 29 46.	7.68	7.52	-40	I
089	UGCA 128	40.3	7.9	13.2	7.3	4.9	-43	06 21 05.52	-20 02 54.6	7.68	7.42	-89	I
090	NGC 2221	47.8	7.5					06 20 15.57	-57 34 40.8	7.61	7.28	23	E
091	ESO 005-G004	97.5	17.9	18.0	3.1	< 1.	-81	06 05 38.2	-86 37 53.	8.36	7.29	26	E
092	ESO 255-IG007	65.7								7.74	7.14	28	E
092	ESO 255-IG007A		40.4	46.1	3.1	2.5	-44	06 27 21.63	-47 10 36.0	7.74	7.14	28	E
092	ESO 255-IG007B		5.6					06 27 22.48	-47 10 46.3	7.74	7.14	28	E
092	ESO 255-IG007C		6.9	10.4	7.0	3.4	-10	06 27 23.06	-47 11 02.4	7.74	7.14	28	E
093	ESO 557-G002	26.7	14.3	19.9	5.2	4.3	43	06 31 47.25	-17 37 17.2	7.79	7.42	35	E
094	NGC 2280	68.5	1.20					06 44 49.08	-27 38 19.0	7.61	7.46	-45	I
095	IRAS 06478-1111	49.7	8.2	42.3	17.3	13.6	-86	06 50 10.64	-11 15 12.8	7.62	7.51	-43	I
096	IRAS F06592-6313	20.3	18.7	19.5	1.7	1.5	-77	06 59 40.07	-63 17 52.8	7.94	7.13	-1	E
097	AM 0702-601	57.0								7.64	7.45	15	E
097	AM 0702-601 N	34.7	30.9	33.2	2.1	1.9	-10	07 03 24.08	-60 15 22.4	7.64	7.45	15	E
097	AM 0702-601 S	22.4	19.6	22.2	2.8	2.6	23	07 03 28.47	-60 16 44.3	7.64	7.45	15	E
098	ESO 491-G020/021	91.2								7.65	7.34	36	E
098	ESO 491-G020	53.5	28.9	41.7	5.3	4.6	-68	07 09 46.87	-27 34 08.1	7.65	7.34	36	E
098	ESO 491-G021	37.5	5.5					07 09 49.89	-27 34 30.0	7.65	7.34	36	E
099	ESO 492-G002	102.	7.1	84.1	26.9	23.0	75	07 11 40.47	-26 42 18.9	7.67	7.38	-86	I
100	NGC 2369	148.	73.0	119.	8.7	3.0	-8	07 16 37.50	-62 20 37.2	7.68	7.48	-25	E
101	ESO 428-G023	53.8	36.4	42.6	3.6	2.6	61	07 22 09.39	-29 14 08.3	7.72	7.37	-85	I
102	NGC 2397	51.4	4.5					07 21 19.60	-69 00 05.3	7.69	7.63	-19	E
103	ESO 428-G028	51.5	5.9					07 23 38.48	-30 03 05.4	7.76	7.39	-77	I
104	IRAS 07251-0248	13.4	12.9	13.3	1.4	1.2	71	07 27 37.63	-02 54 54.6	8.14	7.44	47	E
105	NGC 2442	330.	23.7	32.2	5.2	3.9	49	07 36 23.49	-69 31 51.2	7.89	7.42	-17	E
106	ESO 163-G011/010	57.4								7.55	7.23	0	E
106	ESO 163-G011	51.1	6.8					07 38 05.38	-55 11 27.4	7.55	7.23	0	E
106	ESO 163-G010	6.3	0.94					07 37 53.21	-55 10 58.2	7.55	7.23	0	E
107	ESO 209-G009	122.	2.1					07 58 15.2	-49 51 14.	7.68	7.21	8	E
108	NGC 2525	52.0	4.9	6.3	4.1	4.0	72	08 05 38.06	-11 25 38.1	7.64	7.64	-9	I
109	NGC 2566	142.	63.2	90.0	5.4	4.3	22	08 18 45.63	-25 29 59.0	7.64	7.38	39	I

Table 3 *continued*

Table 3 (*continued*)

Index	Common Name	<i>S</i>	<i>S_P</i>	<i>S_I</i>	ϕ_M	ϕ_m	<i>PA</i>	α	δ	θ_M	θ_m	<i>BPA</i>	
<i>N</i>		(mJy)	(mJy/ Ω_b)	(mJy)	(")	(")	(°)	(J2000)		(")	(")	(°)	Run
(1)	(2)	(3)	(4)	(5)	(6)	(7)	(8)	(9)	(10)	(11)	(12)	(13)	(14)
110	NGC 2613	65.9	0.39					08 33 22.80	-22 58 25.7	7.57	7.47	-49	I
111	IRAS 08355-4944	38.7	30.1	35.9	3.6	3.0	-59	08 37 01.77	-49 54 30.7	7.62	7.47	55	E
112	ESO 432-IG006	46.2								7.60	7.40	37	E
112	ESO 432-IG006 NED01		16.2	23.6	5.7	4.3	-82	08 44 27.21	-31 41 51.4	7.60	7.40	37	E
112	ESO 432-IG006 NED02		11.2	13.1	3.8	2.1	-1	08 44 28.93	-31 41 31.1	7.60	7.40	37	E
113	NGC 2665	30.3	11.5	14.1	3.8	3.4	42	08 46 01.06	-19 18 11.3	7.74	7.46	-90	I
114	ESO 563-G028	61.1	38.0	52.5	5.8	3.5	21	08 50 45.60	-21 57 48.8	7.82	7.46	-88	I
115	ESO 060-IG016	22.8								7.67	7.64	-88	E
115	ESO 060-IG016 NED01		5.9					08 52 30.33	-69 02 00.7	7.67	7.64	-88	E
115	ESO 060-IG016 NED02		15.2					08 52 31.84	-69 01 56.3	7.67	7.64	-88	E
116	NGC 2706	55.7	5.4					08 56 12.31	-02 33 47.0	7.66	7.55	-89	N
117	ESO 564-G011	78.7	26.1	70.9	11.0	8.8	-29	09 02 46.30	-20 43 32.2	7.56	7.53	-49	N
118	IRAS 09022-3615	84.4	81.6	84.1	1.4	1.1	-5	09 04 12.75	-36 27 02.8	8.09	6.91	33	E
119	UGCA 150	48.9	1.5					09 10 49.40	-08 53 26.8	7.56	7.45	-33	N
120	IRAS F09111-1007	47.2								7.58	7.43	-22	N
120	IRAS F09111-1007W	28.2	26.9	28.0	1.6	1.4	42	09 13 36.47	-10 19 29.7	7.58	7.43	-22	N
120	IRAS F09111-1007E	18.7	15.5	17.9	3.2	2.6	52	09 13 38.86	-10 19 19.6	7.58	7.43	-22	N
121	ESO 126-G002	52.8	24.0	34.1	5.4	4.2	-90	09 13 30.16	-60 47 21.3	7.63	7.19	7	F
122	ESO 091-G016	37.6	11.8	32.9	14.0	6.3	-61	09 38 13.45	-63 29 10.2	7.47	7.36	82	F
123	NGC 2992	238.	157.	220.	6.0	3.4	-8	09 45 41.95	-14 19 35.3	7.57	7.54	-25	N
124	NGC 2993	82.7	25.6	76.8	12.6	8.9	42	09 45 48.33	-14 22 05.2	7.57	7.54	-25	N
125	NGC 3059	117.	4.9					09 50 06.6	-73 55 25.	8.16	7.04	14	F
126	IC 2522	56.7	2.5					09 55 08.95	-33 08 13.6	7.53	7.32	15	L
127	NGC 3095	54.6	13.2	15.9	3.7	3.1	-25	10 00 05.84	-31 33 09.5	7.64	7.37	-87	L
128	NGC 3110	131.	23.6	89.8	16.1	9.7	-58	10 04 02.06	-06 28 29.3	7.59	7.59	-5	N
129	ESO 374-IG032	16.3								7.60	7.34	-32	F
129	ESO 374-IG032 NED01	1.5						10 06 03.9	-33 53 20.	7.60	7.34	-32	F
129	ESO 374-IG032 NED02		12.4	13.5	2.7	1.6	-80	10 06 04.65	-33 53 05.0	7.60	7.34	-32	F
130	NGC 3125	25.9								7.55	7.32	5	N
130	NGC 3125A		6.8					10 06 33.35	-29 56 07.0	7.55	7.32	5	N
130	NGC 3125B		4.9					10 06 33.93	-29 56 12.5	7.55	7.32	5	N
131	IC 2554	102.	22.6	57.1	11.1	7.3	53	10 08 49.99	-67 01 53.3	7.42	7.37	-4	F
132	NGC 3175	87.9	6.2	34.6	23.4	10.3	46	10 14 42.11	-28 52 19.4	7.47	7.42	-19	N
133	ESO 500-G034	62.1	49.6	58.2	3.7	2.4	-21	10 24 31.47	-23 33 10.8	7.59	7.28	-2	N
134	ESO 317-G023	82.0	64.8	74.3	3.4	2.2	8	10 24 42.46	-39 18 20.5	7.63	7.34	90	L
135	NGC 3256	729.	187.	587.	12.2	9.3	46	10 27 51.16	-43 54 15.7	7.35	7.33	87	F
136	NGC 3263	146.	16.1	87.1	22.3	10.3	-78	10 29 13.37	-44 07 22.2	7.48	7.40	65	L
137	NGC 3278		62.4					10 31 35.4	-39 57 23.	7.49	7.42	85	L
138	NGC 3281	93.3	70.6	73.1	1.7	1.1	31	10 31 52.08	-34 51 13.1	8.02	7.48	-69	L

Table 3 *continued*

Table 3 (*continued*)

Index <i>N</i> (1)	Common Name (2)	<i>S</i> (mJy) (3)	<i>S_P</i> (mJy/ Ω_b) (4)	<i>S_I</i> (mJy) (5)	ϕ_M ($''$) (6)	ϕ_m ($''$) (7)	<i>PA</i> ($^{\circ}$) (8)	α (J2000) (9)	δ ($''$) (10)	θ_M ($''$) (11)	θ_m ($''$) (12)	<i>BPA</i> ($^{\circ}$) (13)	Run (14)
139	ESO 264-G036	53.0	17.7					10 43 07.67	-46 12 44.3	7.51	7.39	51	F
140	ESO 264-G057	43.7	13.4	26.5	7.9	6.6	-64	10 59 01.81	-43 26 25.3	7.46	7.28	1	F
141	ESO 093-G003	84.9	12.1	49.7	14.7	11.9	-51	10 59 26.03	-66 19 57.3	7.65	7.44	11	F
142	NGC 3508	73.7	11.4					11 02 59.69	-16 17 22.3	7.51	7.48	53	N
143	NGC 3511	78.9	1.28					11 03 23.81	-23 05 12.8	7.53	7.44	-34	N
144	ESO 265-G007	43.8						11 07 48.7	-46 31 37.	7.29	7.18	-3	F
145	ESO 215-G031	42.8	4.8	26.1	18.1	13.0	-84	11 10 34.74	-49 06 09.1	7.38	7.35	-2	F
146	NGC 3568	74.8	5.1					11 10 48.46	-37 26 51.8	7.60	7.32	87	L
147	NGC 3597	80.9	42.1	78.4	8.6	5.3	81	11 14 41.99	-23 43 39.8	7.67	7.30	76	N
148	NGC 3620	194.	136.	169.	4.6	2.7	84	11 16 04.19	-76 12 57.6	7.79	7.52	3	F
149	NGC 3621	258.						11 18 15.2	-32 48 39.	7.66	7.30	73	L
150	CGCG 011-076	39.9	28.9	36.3	4.2	3.6	-80	11 21 12.25	-02 59 02.9	7.64	7.60	0	N
151	NGC 3672	70.5	3.9					11 25 02.48	-09 47 43.3	7.50	7.50	34	N
152	ESO 319-G022	26.5	20.5	22.1	2.3	1.8	-48	11 27 54.07	-41 36 52.0	7.41	7.41	-3	F
153	NGC 3717	80.0	19.7	49.4	14.2	4.5	34	11 31 31.88	-30 18 28.0	7.47	7.43	-2	N
154	NGC 3732	35.6	8.7					11 34 13.95	-09 50 44.9	7.70	7.35	-23	N
155	NGC 3882	185.	7.1					11 46 06.26	-56 23 27.3	7.27	7.22	-3	F
156	NGC 3885	51.2	27.1	47.3	8.4	4.3	-60	11 46 46.45	-27 55 20.6	7.60	7.27	-6	N
157	NGC 3887	43.0	0.61					11 47 04.61	-16 51 16.6	7.48	7.48	-40	N
158	ESO 320-G030	116.	77.8	101.	4.4	3.6	-56	11 53 11.70	-39 07 48.9	7.36	7.32	87	F
159	NGC 3955	54.6	5.1					11 53 57.14	-23 09 49.9	7.47	7.45	-45	N
160	NGC 3981	68.4	5.8					11 56 07.53	-19 53 45.5	7.47	7.46	-51	N
161	NGC 4027	116.						11 59 31.	-19 15 45.	7.54	7.30	-39	N
162	NGC 4030	167.						12 00 23.6	-01 05 55.	8.31	7.16	-35	J
163	NGC 4038/9	590.								7.79	7.40	-48	J
163	NGC 4038		15.2					12 01 53.05	-18 52 03.9	7.79	7.40	-48	J
164	ESO 440-IG058	55.4								7.42	7.39	-3	F
164	ESO 440-IG058 NED01		1.2					12 06 51.7	-31 56 46.	7.42	7.39	-3	F
164	ESO 440-IG058 NED02		33.4	51.7	7.5	3.1	57	12 06 51.92	-31 56 59.3	7.42	7.39	-3	F
165	ESO 267-G030	61.5	26.6	57.6	9.3	6.6	-60	12 14 12.79	-47 13 42.9	7.42	7.27	-1	F
166	IRAS 12116-5615	36.0	32.9	35.2	2.0	1.9	24	12 14 22.01	-56 32 33.0	7.66	7.10	0	F
167	ESO 380-G001	59.1	41.3	50.1	3.8	3.1	32	12 14 45.13	-35 30 35.3	7.56	7.39	-16	L
168	NGC 4219	107.	10.5	32.8	12.3	9.6	45	12 16 27.39	-43 19 27.0	7.56	7.43	-18	L
169	NGC 4304	41.4	12.9	15.5	3.5	3.1	86	12 22 12.73	-33 29 04.6	7.39	7.38	-3	L
170	IRAS F12224-0624	10.4	9.9	10.0	1.0	< 1.	72	12 25 03.91	-06 40 52.4	7.77	7.50	-52	J
171	NGC 4418	39.0	39.3	39.6	0.9	< 1.	-49	12 26 54.62	-00 52 39.1	7.98	7.41	-57	J
172	NGC 4433	134.	37.5					12 27 38.57	-08 16 41.6	7.84	7.80	11	J
173	NGC 4575	76.1	7.2					12 37 51.13	-40 32 14.6	7.52	7.37	9	L
174	IC 3639	94.7	47.8	55.4	3.1	2.8	2	12 40 52.86	-36 45 21.4	7.50	7.34	1	L

Table 3 *continued*

Table 3 (*continued*)

Index <i>N</i> (1)	Common Name (2)	<i>S</i> (mJy) (3)	<i>S_P</i> (mJy/ Ω_b) (4)	<i>S_I</i> (mJy) (5)	ϕ_M ($''$) (6)	ϕ_m ($''$) (7)	<i>PA</i> ($^{\circ}$) (8)	α (J2000) (9)	δ ($''$) (10)	θ_M ($''$) (11)	θ_m ($''$) (12)	<i>BPA</i> ($^{\circ}$) (13)	Run (14)
175	NGC 4666	469.	13.4					12 45 08.63 -00 27 43.4	7.70	7.59	-48	J	
176	NGC 4691	53.3							7.74	7.51	-44	J	
176	NGC 4691A		5.1					12 48 12.73 -03 19 58.5	7.74	7.51	-44	J	
176	NGC 4691B		6.4					12 48 13.89 -03 19 59.7	7.74	7.51	-44	J	
177	NGC 4699	30.8	5.5	6.1	2.8	2.3	71	12 49 02.19 -08 39 51.7	7.83	7.47	-42	J	
178	NGC 4781	98.5						12 54 23.7 -10 32 11.	7.93	7.36	-47	J	
179	IC 3908	71.7	8.5					12 56 40.62 -07 33 44.6	8.09	7.73	-38	J	
180	NGC 4818	50.5	35.9	43.2	3.8	3.2	35	12 56 48.89 -08 31 31.2	7.86	7.69	-84	J	
181	ESO 443-G017	40.7	32.3	38.3	3.7	2.7	45	12 57 44.91 -29 45 58.8	7.64	7.34	-45	J	
182	NGC 4835	203.	6.0					12 58 07.80 -46 15 51.9	7.47	7.37	78	F	
183	MCG -02-33-098/9	35.4							7.59	7.45	40	F	
183	MCG -02-33-098W		15.7					13 02 19.71 -15 46 04.3	7.59	7.45	40	F	
183	MCG -02-33-098		8.8					13 02 20.43 -15 45 59.5	7.59	7.45	40	F	
184	ESO 507-G070	90.0	53.8	57.2	2.3	1.4	71	13 02 52.41 -23 55 18.2	7.49	7.48	-32	F	
185	NGC 4945	6760.	2700.	450.	7.9	4.3	46	13 05 27.53 -49 28 04.8	7.53	7.45	62	B	
186	ESO 323-G077	40.4	27.4	38.0	5.0	4.2	-21	13 06 26.15 -40 24 53.0	7.45	7.43	35	L	
187	IRAS 13052-5711	70.1	67.9	70.0	1.7	0.6	-10	13 08 18.69 -57 27 29.8	7.59	7.29	31	B	
188	NGC 4984	35.2	14.2	24.2	6.7	6.1	28	13 08 57.29 -15 30 59.0	7.83	7.42	-45	J	
189	NGC 5010	80.4	35.2	76.1	11.9	4.4	-58	13 12 26.50 -15 47 51.8	7.67	7.39	87	B	
190	MCG -03-34-014	70.8	6.9					13 12 35.39 -17 32 33.2	7.67	7.62	-52	J	
191	IRAS 13120-5453	326.	326.	334.	1.5	0.5	-45	13 15 06.34 -55 09 22.1	7.59	7.34	-89	B	
192	NGC 5038	57.5	48.5	54.9	3.4	2.0	89	13 15 02.08 -15 57 06.8	7.98	7.37	-42	J	
193	NGC 5054	102.	12.7	43.1	13.8	10.0	-34	13 16 58.44 -16 38 04.8	7.84	7.43	-37	J	
194	NGC 5068	84.7						13 18 54.1 -21 01 59.	7.65	7.26	-10	B	
195	NGC 5073	43.0	27.9	32.1	3.8	2.0	-36	13 19 20.65 -14 50 40.5	7.98	7.47	-42	J	
196	NGC 5078	200.	119.	131.	2.6	2.0	-60	13 19 50.00 -27 24 37.1	8.00	7.13	-50	J	
197	MCG -03-34-064	270.	279.	275.	< 1.			13 22 24.57 -16 43 42.2	7.70	7.51	-39	B	
198	NGC 5128	299000.	4190.	4560.	2.5	1.6	51	13 25 27.64 -43 01 09.3	7.04	6.91	0	L	
199	NGC 5135	214.	150.	190.	4.8	2.7	18	13 25 44.07 -29 50 01.0	7.61	7.40	-10	B	
200	ESO 173-G015	357.	199.	286.	6.0	3.7	-28	13 27 23.83 -57 29 21.7	7.53	7.38	40	B	
201	NGC 5188	108.	68.5	88.8	4.7	3.3	88	13 31 28.28 -34 47 40.4	7.61	7.29	-9	L	
202	IC 4280	64.6	13.8					13 32 53.47 -24 12 25.1	7.62	7.36	90	B	
203	NGC 5236	2800.	65.4	299.	16.3	12.2	-31	13 37 00.55 -29 51 55.5	7.69	7.29	-73	J	
204	NGC 5247	166.						13 38 03.2 -17 53 03.	8.74	7.54	-37	J	
205	NGC 5253	91.5	22.9	59.7	10.4	8.6	8	13 39 55.98 -31 38 26.7	7.63	7.31	0	L	
206	ESO 221-IG008	28.7						13 50 27.6 -48 16 38.	7.43	7.29	-1	B	
207	ESO 221-IG010	116.	17.5	59.2	14.2	9.1	-46	13 50 56.87 -49 03 18.3	7.62	7.32	84	B	
208	NGC 5427	87.8	4.0	14.7	13.9	11.1	46	14 03 26.13 -06 01 50.7	7.96	7.26	-51	J	
209	NGC 5483	37.						14 10 25.0 -43 19 30.	7.59	7.34	-90	B	

Table 3 *continued*

Table 3 (*continued*)

Index	Common Name	<i>S</i>	<i>S_P</i>	<i>S_I</i>	ϕ_M	ϕ_m	<i>PA</i>	α	δ	θ_M	θ_m	<i>BPA</i>	
<i>N</i>	Name	(mJy)	(mJy/ Ω_b)	(mJy)	($''$)	($''$)	($^{\circ}$)	(J2000)		($''$)	($''$)	($^{\circ}$)	Run
(1)	(2)	(3)	(4)	(5)	(6)	(7)	(8)	(9)	(10)	(11)	(12)	(13)	(14)
210	ESO 221-G032	62.5						14 12 09.25	-49 23 22.2	7.40	7.36	-2	B
211	NGC 5506	360.	335.	347.	1.6	1.5	-62	14 13 14.95	-03 12 27.7	7.86	7.71	-34	J
212	IC 4402	51.7	20.6	25.8	4.4	3.0	-44	14 21 13.10	-46 17 52.0	7.56	7.42	-41	B
213	NGC 5595	124.	5.9					14 24 13.34	-16 43 21.1	7.69	7.34	-53	J
214	NGC 5597	68.9	12.2	26.4	10.2	5.9	45	14 24 27.53	-16 45 46.8	7.69	7.34	-53	J
215	IC 4444	245.	11.7					14 31 38.8	-43 25 10.	7.52	7.43	44	L
216	NGC 5643	234.	20.4					14 32 40.75	-44 10 28.7	7.54	7.26	-1	L
217	IRAS F14348-1447	37.4	32.0	37.1	4.3	1.4	42	14 37 38.32	-15 00 22.6	8.36	7.52	-18	G
218	NGC 5713	176.	22.7					14 40 11.3	-00 17 20.	8.19	7.89	-33	G
219	IRAS F14378-3651	31.6	30.9	30.9	1.0	< 1.0	31	14 40 59.07	-37 04 32.0	7.57	7.33	32	B
220	NGC 5719	64.1	25.1	50.5	11.0	5.1	-85	14 40 56.35	-00 19 05.4	8.19	7.89	-33	G
221	NGC 5728	82.3	32.7	52.4	7.1	5.2	-55	14 42 23.79	-17 15 09.6	8.66	7.36	-5	G
222	NGC 5734	78.0	18.8					14 45 09.13	-20 52 13.3	7.50	7.46	45	B
223	ESO 386-G019	34.5	17.2	33.5	8.0	6.4	-10	14 46 10.41	-37 41 06.4	7.50	7.23	0	L
224	UGCA 394	36.1	6.3	17.6	16.7	5.5	-13	14 47 24.17	-17 26 45.1	8.80	7.20	-47	G
225	NGC 5757	48.9	12.8	21.3	7.4	5.2	-18	14 47 46.38	-19 04 42.5	7.88	7.66	-14	G
226	IC 4518A/B	176.								7.50	7.49	72	B
226	IC 4518A		88.6	149.	9.3	2.6	83	14 57 41.24	-43 07 55.5	7.50	7.49	72	B
226	IC 4518B		6.2	19.0	18.8	3.9	-78	14 57 44.95	-43 07 55.0	7.50	7.49	72	B
227	NGC 5786	70.6	12.6	27.6	10.2	6.1	48	14 58 56.38	-42 00 49.1	7.50	7.41	31	L
228	NGC 5792	78.1	15.2	36.5	15.2	3.8	79	14 58 22.69	-01 05 27.9	8.71	7.59	-34	G
229	NGC 5793	1020.	1070.	1040.	< 1.	< 1.		14 59 24.75	-16 41 35.8	9.42	6.86	-17	G
230	NGC 5861	78.4	3.9					15 09 16.14	-11 19 18.1	9.65	6.91	-13	G
231	NGC 5833	74.5	6.1					15 11 53.43	-72 51 33.6	7.83	7.40	-38	B
232	UGCA 402	63.6	4.3					15 13 30.94	-20 40 28.8	7.95	7.63	-30	G
233	NGC 5915	70.8	13.7					15 21 33.5	-13 05 33.	8.30	8.05	-40	G
234	ESO 099-G004	64.1	38.5	61.9	7.8	3.7	-11	15 24 57.95	-63 07 31.7	7.51	7.40	-4	B
235	NGC 5937	123.	19.1					15 30 46.09	-02 49 45.9	8.36	7.61	-48	G
236	NGC 6000	187.	93.2	117.	4.5	3.3	3	15 49 49.51	-29 23 13.1	7.88	7.53	-40	G
237	ESO 137-G014	36.4	23.4	31.4	4.9	3.9	-89	16 17 10.79	-58 18 45.9	7.87	7.32	-68	B
238	IC 4595	79.9	6.6					16 20 44.03	-70 08 34.9	8.12	7.20	-54	B
239	IRAS F16164-0746	69.6	70.1	70.5	1.9	< 1.	-18	16 19 11.78	-07 54 03.0	8.92	7.04	-11	G
240	ESO 452-G005	53.3	10.1					16 31 40.17	-28 06 07.6	7.73	7.53	-44	G
241	NGC 6156	176.	11.4					16 34 52.53	-60 37 06.5	7.45	7.33	-2	A
242	ESO 069-IG006	54.2	47.7	54.6	3.7	1.8	-39	16 38 11.79	-68 26 06.9	7.80	7.24	1	A
243	IRAS F16399-0937	60.9	28.8	57.8	8.5	6.5	27	16 42 40.14	-09 43 12.8	7.66	7.39	-23	A
244	ESO 453-G005	30.0	23.5	25.9	3.0	1.6	33	16 47 31.11	-29 21 19.9	7.54	7.32	0	A
245	NGC 6215	327.	12.5					16 51 06.67	-58 59 33.3	7.52	7.23	0	A
246	NGC 6221	386.	43.6	90.9	8.5	6.9	85	16 52 46.20	-59 12 59.3	7.47	7.29	-1	A

Table 3 *continued*

Table 3 (*continued*)

Index	Common Name	<i>S</i>	<i>S_P</i>	<i>S_I</i>	ϕ_M	ϕ_m	<i>PA</i>	α	δ	θ_M	θ_m	<i>BPA</i>	
<i>N</i>		(mJy)	(mJy/ Ω_b)	(mJy)	(")	(")	(°)			(")	(")	(°)	Run
(1)	(2)	(3)	(4)	(5)	(6)	(7)	(8)	(9)	(10)	(11)	(12)	(13)	(14)
247	IRAS F16516–0948	83.2	20.7	76.9	13.9	10.9	59	16 54 23.98	-09 53 19.9	7.56	7.46	-32	A
248	NGC 6300	111.	14.5	16.2	2.9	2.3	16	17 16 59.40	-62 49 12.4	7.54	7.29	-1	A
249	IRAS F17138–1017	69.0	49.4	67.3	5.7	3.2	5	17 16 35.85	-10 20 41.3	7.63	7.50	27	G
250	IRAS F17207–0014	107.	103.	105.	1.	0.9	-46	17 23 22.02	-00 17 01.8	7.83	7.47	27	G
251	ESO 138-G027	55.7	22.0	36.6	6.2	5.8	58	17 26 43.21	-59 55 54.1	7.52	7.24	0	A
252	IC 4662	30.1						17 47 07.8	-64 38 28.	7.58	7.24	0	A
253	IRAS 17578–0400	76.3	61.7	69.4	3.0	2.3	-67	18 00 31.89	-04 00 52.1	7.58	7.54	-33	A
253	IRAS 17578–0400W	29.0	5.9	24.9	15.9	11.5	59	18 00 24.52	-04 01 00.9	7.58	7.54	-33	A
253	IRAS 17578–0400S	15.2	5.8	12.2	8.9	7.0	71	18 00 34.01	-04 01 43.3	7.58	7.54	-33	A
254	IC 4687/6	112.								7.47	7.23	0	A
254	IC 4686	11.5	9.9	10.6	2.0	1.9	-33	18 13 38.63	-57 43 56.2	7.47	7.23	0	A
254	IC 4687	99.8	45.4	91.2	8.2	6.5	81	18 13 39.57	-57 43 30.5	7.47	7.23	0	A
255	ESO 140-G012	33.5	13.3	18.9	5.1	4.5	3	18 14 16.72	-60 05 29.2	7.67	7.09	0	A
256	IRAS F18293–3413	233.	145.	222.	5.9	4.9	-60	18 32 41.12	-34 11 26.7	7.52	7.19	0	A
257	IC 4734	80.4	52.3	62.7	3.8	2.6	-74	18 38 25.55	-57 29 24.4	7.65	7.09	0	A
258	NGC 6744	227.	0.26					19 09 45.94	-63 51 26.7	7.84	7.12	-3	A
259	NGC 6753	148.	9.1					19 11 23.55	-57 02 56.3	7.64	7.14	-1	A
260	ESO 593-IG008	69.0	39.0	63.4	7.6	4.2	20	19 14 31.18	-21 19 07.4	7.70	7.17	4	A
261	IRAS F19297–0406	32.8	30.6	32.6	2.5	1.2	-39	19 32 22.32	-04 00 02.6	7.76	7.63	37	G
262	NGC 6808	96.9	6.6					19 43 53.68	-70 38 00.2	7.92	7.26	-42	A
263	NGC 6810	144.	22.2	92.4	17.5	9.6	-19	19 43 34.31	-58 39 20.6	7.62	7.30	-3	A
264	NGC 6814	72.5	6.6	7.1	2.3	2.0	22	19 42 40.60	-10 19 26.6	7.75	7.68	47	G
265	NGC 6822	100.						19 44 51.4	-14 47 35.	7.58	7.57	43	D
266	NGC 6835	56.1	30.3	47.3	7.2	4.1	67	19 54 32.90	-12 34 05.1	7.72	7.60	-12	G
267	ESO 339-G011	164.	134.	146.	2.5	2.0	56	19 57 37.68	-37 56 08.6	8.07	7.07	48	D
268	IC 4946	17.0	14.4	16.2	3.1	2.2	69	20 23 58.16	-43 59 41.3	8.05	6.99	48	K
269	NGC 6907	155.	17.4	44.0	9.5	6.1	-70	20 25 06.78	-24 48 33.9	7.56	7.43	44	D
270	NGC 6918	38.2	31.2	36.0	3.3	2.4	-13	20 30 47.19	-47 28 25.5	7.66	7.29	41	D
271	NGC 6926	127.	13.4	36.7	10.4	9.7	-22	20 33 06.30	-02 01 39.0	7.66	7.61	5	D
272	IC 5063	1490.	1370.	1430.	1.6	1.6		20 52 02.21	-57 04 07.3	7.69	7.37	49	D
273	ESO 286-IG019	33.3	29.0	31.6	2.4	2.1	-53	20 58 26.90	-42 39 00.8	7.56	7.52	45	D
274	ESO 286-G035	49.0	30.8	46.4	7.0	3.5	12	21 04 11.21	-43 35 36.2	8.03	6.93	39	D
275	ESO 402-G026	40.0	18.8	29.7	7.0	4.3	-74	21 22 31.43	-36 40 52.6	7.48	7.44	-39	K
276	NGC 7083	69.3						21 35 45.2	-63 54 08.	8.02	7.11	41	D
277	NGC 7090	54.5						21 36 30.1	-54 33 35.	7.81	7.18	38	D
278	ESO 343-IG013	29.2								8.02	6.98	37	D
278	ESO 343-IG013 NED01		11.6	21.1	7.2	4.1	-86	21 36 10.71	-38 32 43.3	8.02	6.98	37	D
278	ESO 343-IG013 NED02			5.3				21 36 11.02	-38 32 34.2	8.02	6.98	37	D
279	NGC 7130	196.	146.	164.	2.9	2.3	3	21 48 19.66	-34 57 05.2	7.75	7.31	44	D

Table 3 *continued*

Table 3 (*continued*)

Index <i>N</i> (1)	Common Name (2)	<i>S</i> (mJy) (3)	<i>S_P</i> (mJy/ Ω_b) (4)	<i>S_I</i> (mJy) (5)	ϕ_M ($''$) (6)	ϕ_m ($''$) (7)	<i>PA</i> ($^{\circ}$) (8)	α (J2000) (9)	δ ($''$) (10)	θ_M ($''$) (11)	θ_m ($''$) (12)	<i>BPA</i> ($^{\circ}$) (13)	Run (14)
280	NGC 7172	38.0	17.1	33.1	10.6	3.8	-88	22 02 01.93 -31 52 10.0	7.51	7.49	-70	K	
281	NGC 7205	95.9						22 08 34.4 -57 26 36.	7.82	7.23	37	D	
282	ESO 467-G027	58.7	7.5					22 14 40.00 -27 27 49.4	7.59	7.52	-37	H	
283	IC 5179	180.	27.2					22 16 09.24 -36 50 37.7	8.00	6.92	43	D	
284	ESO 602-G025	51.7	28.1	40.4	5.7	4.2	-8	22 31 25.51 -19 02 03.4	7.78	7.16	-24	H	
285	ESO 534-G009	73.8	54.3	61.6	3.4	2.0	33	22 38 41.39 -25 51 01.5	7.62	7.36	-38	H	
286	ESO 239-IG002	44.2	38.5	41.6	2.6	1.6	16	22 49 39.97 -48 50 59.2	7.59	7.17	1	D	
287	IRAS F22491-1808	6.7	6.1	6.7	2.7	0.6	-69	22 51 49.33 -17 52 23.3	7.70	7.21	-15	H	
288	NGC 7418	54.8	1.7					22 56 36.16 -37 01 47.4	8.12	7.34	34	K	
289	NGC 7496	46.3	16.9	20.1	3.7	2.7	-34	23 09 47.31 -43 25 40.1	7.64	7.20	-4	K	
290	ESO 148-IG002	34.8	26.2	33.5	5.6	1.7	-2	23 15 46.86 -59 03 15.7	7.64	7.13	1	D	
291	NGC 7552	332.	116.	222.	7.3	7.1	41	23 16 10.85 -42 35 06.2	8.07	6.95	45	D	
292	NGC 7582	326.	156.	209.	5.2	3.4	-34	23 18 23.65 -42 22 13.0	7.59	7.27	17	K	
293	NGC 7592	79.8							7.64	7.54	-22	H	
293	NGC 7592A		32.3	44.5	5.9	3.3	-64	23 18 21.85 -04 24 56.4	7.64	7.54	-22	H	
293	NGC 7592B		20.5	39.7	9.3	5.3	84	23 18 22.58 -04 24 58.0	7.64	7.54	-22	H	
293	NGC 7592C			2.1				23 18 22.1 -04 25 09.	7.64	7.54	-22	H	
294	NGC 7590	75.4		2.1				23 18 54.9 -42 14 22.	7.59	7.27	17	K	
295	NGC 7599	65.6						23 19 20.8 -42 15 30.	7.59	7.27	17	K	
296	ESO 077-IG014	44.4							7.68	7.62	-29	D	
296	ESO 077-IG014 NED01		10.9	11.6	2.3	1.4	87	23 21 03.69 -69 13 02.0	7.68	7.62	-29	D	
296	ESO 077-IG014 NED02		30.7	31.7	1.5	1.2	46	23 21 05.42 -69 12 48.3	7.68	7.62	-29	D	
297	MCG -01-60-022	55.0	24.8	45.8	8.3	5.7	-63	23 42 01.01 -03 36 55.5	7.81	7.54	25	D	
298	NGC 7793		127.					23 57 48.4 -32 35 27.	7.61	7.37	-90	K	

NOTE—Table 3 is published in its entirety in the machine-readable format.

3.4. Notes on individual sources

001: *NGC 0034*.—Marginally detected extremely faint ($\langle S_P \rangle \sim 15 \mu\text{Jy beam}^{-1}$) double-lobed emission with LAS $\approx 13'$ in PA $\approx 48^{\circ}$ is centered on the unresolved radio core. Late-stage merger galaxy (Fernández et al. 2010).

002: *NGC 0055*.—The radio emission from this edge-on galaxy has LAS = 28' in PA = -73°. The brightest radio component listed in Table 3 at $\alpha = 00^{\text{h}} 14^{\text{m}} 57^{\text{s}}.54$, $\delta = -39^{\circ} 12' 25''.8$ coincides with the brightest nearby *WISE* source ($W_1 = 9.459$, $W_2 = 9.319$, $W_3 = 5.312$) at $\alpha = 00^{\text{h}} 14^{\text{m}} 57^{\text{s}}.60$, $\delta = -39^{\circ} 12' 25''.5$. This may be the actual obscured nucleus of NGC 0055, despite

being significantly offset from the 2MASX position $\alpha = 00^{\text{h}} 14^{\text{m}} 53^{\text{s}}.60$, $\delta = -39^{\circ} 11' 47''.9$ preferred by NED.

004: *NGC 0134*.—The radio source LAS = 7' in PA = 48°.

007: *NGC 0157*.—No visible radio nucleus.

008: *ESO 350-IG038*.—Compact group of galaxies (Schmitt et al. 2006) only marginally resolved by MeerKAT. Warm $\alpha(25 \mu\text{m}, 60 \mu\text{m}) = -1.15$ suggests a significant AGN contribution to the *IRAS* source (de Grijp et al. 1985).

010: *NGC 0232*.—The companion galaxy NGC 0230 is a $S = 9.5 \text{ mJy}$ radio source with FWHM size $\phi_M = 16''.0$ and $\phi_m = 4''.9$ in PA = 43° centered on $\alpha = 00^{\text{h}} 42^{\text{m}} 27^{\text{s}}.14$, $\delta = -23^{\circ} 37' 43''.44$. The companion galaxy NGC 0232E is an unresolved radio source with $S = 39.2 \text{ mJy}$ at $\alpha = 00^{\text{h}} 42^{\text{m}} 52^{\text{s}}.83$, $\delta = -23^{\circ} 32' 27''.4$.

011: *NGC 0247*.—Extremely diffuse and patchy galaxy, marginal radio detection, very uncertain total flux density and position.

012: *NGC 0253*.—The radio source LAS = $19'$ in PA = 49° .

014: *NGC 0300*.—Very faint patchy radio source, no visible nucleus, very uncertain total flux density and position. LAS $\sim 17'$.

021: *NGC 0625*.—The radio continuum from this dwarf starburst galaxy is primarily free-free emission (Cannon & Skillman 2004). The MeerKAT position is for the brightest of three H II regions, about $2''$ east of the galaxy centroid.

026: *NGC 0835*.—The nearby galaxy NGC 0833 is a 4.3 mJy compact radio source at $\alpha = 02^h 09^m 20^s.84$, $\delta = -10^\circ 07' 59''.6$ and may contribute to the *IRAS* source.

031: *NGC 0922*.—Collisional ring galaxy (Elagali et al. 2018), cometary morphology with bright eastern rim. The nucleus is offset to the northeast.

035: *NGC 1068*.—Warm $\alpha(25\ \mu\text{m}, 60\ \mu\text{m}) = -0.92$ and low $q = 1.72$ indicate a dominant AGN contribution (de Grijp et al. 1985) to the radio flux of this starburst galaxy.

038: *NGC 1087*.—The compact $S = 12$ mJy source at $\alpha = 02^h 46^m 29^s.28$, $\delta = -00^\circ 29' 52''.0$ superimposed on the eastern edge of NGC 1087 appears to be an unrelated background source.

039: *NGC 1097*.—Circumnuclear radio ring (Hummel et al. 1987). The MeerKAT central brightness $S_p = 15$ mJy beam $^{-1}$ is less than the $S_p = 21$ mJy beam $^{-1}$ of the surrounding ring, so the Gaussian fitted angular size is an overestimate.

043: *NGC 1232*.—The center of the radio image is empty, with no detectable nucleus.

045: *NGC 1313*.—No clear radio nucleus, very uncertain position.

046: *NGC 1309*.—No clear radio nucleus, very uncertain position. The compact $S_p = 3.4$ mJy beam $^{-1}$ source at $\alpha = 03^h 22^m 06^s.3$, $\delta = -15^\circ 23' 18''$ behind the north edge of NGC 1309 is not included in the flux density.

048: *IC 1953*.—Compact radio core surrounded by a faint circular halo.

050: *NGC 1377*.—Exceptionally faint radio source ($q = 4.33$). The marginally resolved radio continuum extends parallel to the molecular jet (Aalto et al. 2020).

051: *NGC 1386*.—Faint radio disk or jets lie nearly perpendicular to the 2MASX stellar disk.

058: *NGC 1511*.—Fitted position may not be the actual nucleus. Bright eastern radio arc.

059: *NGC 1532*.—Thin edge-on disk with perpendicular radio plumes suggesting outflows. Interacting with

NGC 1531, an $S = 2.4$ mJy source at $\alpha = 04^h 59^m 59^s.26$, $\delta = -32^\circ 51' 04''.2$ with FWHM size $16''.9 \times 14''.5$ in PA = -57°

061: *NGC 1546*.—The optically faint compact $S = 35$ mJy source at $\alpha = 04^h 14^m 35^s.31$, $\delta = -56^\circ 03' 44''.2$ is not included in the NGC 5146 flux density.

062: *IC 2056*.—Radio ring with central hole on the position of the 2MASX stellar nucleus.

063: *NGC 1559*.—Bright, patchy radio emission from the spiral arms, no clearcut nucleus.

064: *NGC 1566*.—Bright, compact Seyfert 1 nucleus and clear spiral arms.

065: *ESO 550-IG025*.—Merging pair of galaxies.

067: *NGC 1614*.—Late-stage merger. A faint ($S_p < 0.1$ mJy beam $^{-1}$) curved tail about $2'$ long and $\leq 7''$ east of NGC 1614 contributes $S \approx 4$ mJy to the flux density, and the base of the straight tail in PA $\approx -150^\circ$ is also visible.

068: *ESO 485-G003*.—The companion edge-on disk galaxy ESO 485-G004 with flux density $S = 3.3$ mJy at $\alpha = 04^h 39^m 06^s.39$, $\delta = -24^\circ 11' 03''.3$ probably contributes to the *IRAS* source.

071: *ESO 203-IG001*.—Completely unresolved radio source, FWHM $< 1''$.

076: *NGC 1792*.—The FRII source at $\alpha = 04^h 20^m 15^s.16$, $\delta = -54^\circ 53' 46''.3$ has no bright optical counterpart and is probably an unrelated background galaxy.

079: *NGC 1832*.—The compact $S = 4.5$ mJy source at $\alpha = 05^h 12^m 03^s.50$, $\delta = -15^\circ 41' 32''.7$ appears to be an unrelated background source and was not included in the flux density of NGC 1832.

082: *NGC 1964*.—No distinct radio nucleus is visible in the bright central region.

083: *NGC 2076*.—No radio nucleus.

084: *NGC 2139*.—No distinct radio nucleus.

087: *NGC 2207/IC 2163*.—Table 1 in Sanders et al. (2003) lists the identification of IRAS F06142–2121 as IC 2163 only, but at a position closer to that of NGC 2207. Our 1.28 GHz MeerKAT image suggests that F06142–2121 is a blend of both galaxies in this merging pair. Our total 1.28 GHz flux density $S = 371$ mJy includes both NGC 2207 and IC 2163 but excludes the apparently unrelated $S = 8$ mJy compact source overlapping the western edge of NGC 2207 at $\alpha = 06^h 16^m 15^s.90$, $\delta = -21^\circ 22' 03''.1$.

088: *UGCA 127*.—There are several bright spots near the center of UGCA 127, but none is clearly the nucleus.

090: *NGC 2221*.—Interacting pair with NGC 2222, $S = 15.8$ mJy at $\alpha = 06^h 20^m 16^s.99$, $\delta = -57^\circ 32' 04''.4$.

091: *ESO 005-G004*.—The MeerKAT nuclear position $\alpha = 06^h 05^m 38^s.2$, $\delta = -86^\circ 37' 53''$ formally ap-

pears to be offset from the 2MASX coadd position $\alpha = 06^{\text{h}} 05^{\text{m}} 41\overset{\text{s}}{.}36$, $\delta = -86^{\circ} 37' 54\overset{\text{s}}{.}2$. However, it is very near the south celestial pole and is probably inaccurate.

- 092: *ESO 255-IG007*.—Tight galaxy triplet.
- 093: *ESO 557-G002*.—Pair with ESO 557-G001, $S = 11.3 \text{ mJy}$ at $\alpha = 06^{\text{h}} 31^{\text{m}} 45\overset{\text{s}}{.}73$, $\delta = -17^{\circ} 38' 47\overset{\text{s}}{.}5$.
- 097: *AM 0702-601*.—Pair of compact galaxies.
- 098: *ESO 491-G020/021*.—Interacting pair of galaxies.
- 099: *ESO 492-G002*.—Pair with ESO 492-G003, $S = 4.6 \text{ mJy}$ at $\alpha = 07^{\text{h}} 11^{\text{m}} 45\overset{\text{s}}{.}01$, $\delta = -26^{\circ} 39' 30\overset{\text{s}}{.}3$.
- 101: *ESO 428-G023*.—The $S_p = 3.2 \text{ mJy beam}^{-1}$ source at $\alpha = 07^{\text{h}} 22^{\text{m}} 06\overset{\text{s}}{.}39$, $\delta = -29^{\circ} 14' 04\overset{\text{s}}{.}2$ is optically faint and probably an unrelated background galaxy.
- 105: *NGC 2442*.—Large open spiral with polarized continuum wisps extending east from the stellar image (Harnett et al. 2004), relatively radio loud ($q = 1.96$).
- 108: *NGC 2525*.—The optically bright stellar bar is not visible in the MeerKAT image.
- 112: *ESO 432-IG006*.—Tidally interacting pair of galaxies.
- 115: *ESO 060-IG016*.—Close pair of galaxies.
- 117: *ESO 564-G011*.—Our flux density $S = 78.7 \text{ mJy}$ does not include the $S = 5.3 \text{ mJy}$ companion galaxy ESO 564-G010 at $\alpha = 09^{\text{h}} 02^{\text{m}} 45\overset{\text{s}}{.}20$, $\delta = -20^{\circ} 42' 49\overset{\text{s}}{.}7$, which may contribute to the *IRAS* source.
- 120. *IRAS F09111-1007*.—The *IRAS* source is a blend of the two galaxies *IRAS F09111-1007W* and *IRAS F09111-1007E*.
- 123. *NGC 2992*.—Interacting pair with NGC 2993.
- 124. *NGC 2993*.—Interacting pair with NGC 2992.
- 125. *NGC 3059*.—The $S = 117 \text{ mJy}$ flux density excludes the compact 6.8 mJy source at $\alpha = 09^{\text{h}} 50^{\text{m}} 18\overset{\text{s}}{.}77$, $\delta = -73^{\circ} 55' 30\overset{\text{s}}{.}2$. Confusing radio source near the nucleus?
- 126. *IC 2522*.—The $S = 56.7 \text{ mJy}$ flux density excludes the 25 mJy companion galaxy IC 2523 at $\alpha = 09^{\text{h}} 55^{\text{m}} 09\overset{\text{s}}{.}54$, $\delta = -33^{\circ} 12' 37\overset{\text{s}}{.}0$.
- 127. *NGC 3095*.—NGC 3095 is a member of the NGC 3100 ($S = 614 \text{ mJy}$ at $\alpha = 10^{\text{h}} 00^{\text{m}} 40\overset{\text{s}}{.}84$, $\delta = -31^{\circ} 39' 51\overset{\text{s}}{.}6$) group.
- 128. *NGC 3110*.—The $S = 131 \text{ mJy}$ flux density includes neither the 6.4 mJy companion galaxy MCG -01-26-013 at $\alpha = 10^{\text{h}} 03^{\text{m}} 57\overset{\text{s}}{.}05$, $\delta = -06^{\circ} 29' 47\overset{\text{s}}{.}6$ nor the small nearby source at $\alpha = 10^{\text{h}} 04^{\text{m}} 00\overset{\text{s}}{.}05$, $\delta = -06^{\circ} 28' 17\overset{\text{s}}{.}5$.
- 129. *ESO 374-IG032*.—This galaxy pair is the correct identification of the *IRAS* source F10038-3338, which had been incorrectly identified with IC 2545.

130. *NGC 3125*.—Blue compact dwarf galaxy. Two bright areas are resolved in both the 2MASX *JHK_s* stellar image and in our 1.28 GHz MeerKAT image.

136. *NGC 3263*.—Long eastern radio tail. Interacting pair with the radio-quiet galaxy NGC 3262 at $\alpha = 10^{\text{h}} 29^{\text{m}} 06\overset{\text{s}}{.}23$, $\delta = -44^{\circ} 09' 34\overset{\text{s}}{.}8$, member of the NGC 3256 group.

137. *NGC 3278*.—Cometary radio morphology brightest on the northwestern edge. No visible radio nucleus.

138. *NGC 3281*.—Radio jets extend perpendicular to the disk of this radio-loud ($q = 1.99$) Seyfert 2 galaxy

140. *ESO 264-G057*.—Brightest in group including ESO 264-G058 ($S = 6.0 \text{ mJy}$ at $\alpha = 10^{\text{h}} 59^{\text{m}} 06\overset{\text{s}}{.}9$, $\delta = -43^{\circ} 22' 34\overset{\text{s}}{.}$) and WISEA J105911.26-432826.7 ($S = 3.8 \text{ mJy}$ at $\alpha = 10^{\text{h}} 59^{\text{m}} 11\overset{\text{s}}{.}4$, $\delta = -43^{\circ} 28' 29\overset{\text{s}}{.}$).

143. *NGC 3511*.—Pair with NGC 3513 ($S = 21.1 \text{ mJy}$ at $\alpha = 11^{\text{h}} 03^{\text{m}} 46\overset{\text{s}}{.}3$, $\delta = -23^{\circ} 14' 45\overset{\text{s}}{.}$).

144. *ESO 265-G007*.—No visible radio nucleus.

146. *NGC 3568*.—Large (LAS = $19'$) tailed $S = 1.01 \text{ Jy}$ radio galaxy NGC 3557 superimposed.

149. *NGC 3621*.—Patchy irregular galaxy with no recognizable radio nucleus.

150. *CGCG 011-076*.—The $S = 39.9 \text{ mJy}$ flux density does not include the possibly interacting companion galaxy LCRS B111835.0-024314 ($S = 1.2 \text{ mJy}$ at $\alpha = 11^{\text{h}} 21^{\text{m}} 08\overset{\text{s}}{.}29$, $\delta = -02^{\circ} 59' 39\overset{\text{s}}{.}4$).

153. *NGC 3717*.—Pair with IC 2913 ($S = 9.8 \text{ mJy}$ at $\alpha = 11^{\text{h}} 31^{\text{m}} 51\overset{\text{s}}{.}2$, $\delta = -30^{\circ} 24' 41\overset{\text{s}}{.}$).

161. *NGC 4027*.—No clearcut radio nucleus.

162. *NGC 4030*.—No visible radio nucleus.

163. *NGC 4038/9*.—NGC 4039 has no clearcut radio nucleus.

164. *ESO 440-IG058*.—Interacting pair of galaxies.

165. *ESO 267-G030*.—Pair with ESO 267-G029 ($S = 30.9 \text{ mJy}$ at $\alpha = 12^{\text{h}} 13^{\text{m}} 52\overset{\text{s}}{.}23$, $\delta = -47^{\circ} 16' 25\overset{\text{s}}{.}6$).

171. *NGC 4418*.—Seyfert 2 galaxy. Radio source FWHM < $1''$ and unusually high $q = 3.12$ suggest this radio source is AGN dominated.

172. *NGC 4433*.—Pair with NGC 4428 ($S = 52.0 \text{ mJy}$ at $\alpha = 12^{\text{h}} 27^{\text{m}} 24\overset{\text{s}}{.}09$, $\delta = -08^{\circ} 10' 52\overset{\text{s}}{.}2$).

174. *IC 3639*.—Seyfert 2 galaxy with companion galaxies ESO 381-G006 ($S = 0.8 \text{ mJy}$ at $\alpha = 12^{\text{h}} 40^{\text{m}} 40\overset{\text{s}}{.}79$, $\delta = -36^{\circ} 44' 21\overset{\text{s}}{.}5$) and ESO 381-G009 ($S = 15.7 \text{ mJy}$ at $\alpha = 12^{\text{h}} 40^{\text{m}} 58\overset{\text{s}}{.}34$, $\delta = -36^{\circ} 43' 54\overset{\text{s}}{.}0$).

175. *NGC 4666*.—Edge-on spiral galaxy with radio emission extending well above and below the disk.

176. *NGC 4691*.—There are two brightness peaks in the MeerKAT radio image, which we labeled NGC 4691A and NGC 4691B.

177. *NGC 4699*.—Compact radio core surrounded by a very faint ($\sim 0.1 \text{ mJy beam}^{-1}$) halo with FWHM = $3'$.

178. *NGC 4781*.—No detectable radio nucleus.
183. *MCG -02-33-098/9*.—IRAS F12596–1529 is a blend of MCG -02-33-098W and MCG -02-33-098. MCG -02-33-099 is radio quiet
193. *NGC 5054*.—Interacting pair with MCG -03-34-040 ($S_p = 0.2 \text{ mJy beam}^{-1}$ at $\alpha = 13^{\text{h}} 16^{\text{m}} 56^{\text{s}}.2$, $\delta = -16^{\circ} 35' 31''$).
194. *NGC 5068*.—Diffuse source with no visible radio nucleus.
196. *NGC 5078*.—Edge-on disk with symmetric perpendicular radio jets or winds originating in the nucleus.
197. *MCG -03-34-064*.—AGN emission dominates the radio emission from this unresolved radio-loud ($q = 1.47$) warm [$\alpha(25 \mu\text{m}, 60 \mu\text{m}) = -0.84$] Seyfert 1.8 galaxy.
198. *NGC 5128*.—Cen A radio galaxy.
203. *NGC 5236*.—M83.
204. *NGC 5247*.—No clearcut radio nucleus.
206. *ESO 221-IG008*.—Marginally resolved pair of galaxies.
208. *NGC 5427*.—Pair with NGC 5426 ($S = 45 \text{ mJy}$, $3'$ south, no visible radio nucleus).
209. *NGC 5483*.—Central bulge but no visible nucleus. Flux density excludes three compact sources on the northwest side.
211. *NGC 5506*.—The strong ($q = 1.48$) compact radio source in this warm [$\alpha(25 \mu\text{m}, 60 \mu\text{m}) = -0.80$] Seyfert 1.9 nucleus is probably dominated by AGN emission.
213. *NGC 5595*.—Pair with NGC 5597.
214. *NGC 5597*.—Pair with NGC 5595.
215. *IC 4444*.—IC 4444 = IC 4441.
218. *NGC 5713*.—Interacting pair with NGC 5719. Indistinct offset radio nucleus.
220. *NGC 5719*.—Interacting pair with NGC 5713.
222. *NGC 5734*.—Pair with NGC 5734S ($S = 58.3 \text{ mJy}$ at $\alpha = 14^{\text{h}} 45^{\text{m}} 11^{\text{s}}.15$, $\delta = -20^{\circ} 54' 49''$).
226. *IC 4518A/B*.—Interacting galaxy pair, possible AGN contribution to the relatively loud ($q = 1.85$) radio source.
228. *NGC 5792*.—The $S = 78.1 \text{ mJy}$ flux density excludes the $S = 5.5 \text{ mJy}$ compact source at $\alpha = 14^{\text{h}} 58^{\text{m}} 51^{\text{s}}.49$, $\delta = -42^{\circ} 00' 34''$.
229. *NGC 5793*.—Seyfert 2, strong ($q = 0.96$) flat-spectrum radio source OQ 194 dominated by AGN emission, near NGC 5796.
233. *NGC 5915*.—Triplet with NGC 5916 and NGC 5916A.
234. *ESO 099-IG004*.—Marginally resolved interacting pair of galaxies?
240. *ESO 452-G005*.—Pair with ESO 452-G007 ($S = 19.3 \text{ mJy}$ at $\alpha = 16^{\text{h}} 32^{\text{m}} 03^{\text{s}}.28$, $\delta = -28^{\circ} 05' 36''$).
- There is no published *IRAS* $\lambda = 100 \mu\text{m}$ flux density for this source.
243. *IRAS F16399–0937*.—Marginally resolved pair of galaxies.
244. *ESO 453-G005*.—Pair with WISEA J164729.33–291906.6 ($S = 14.6 \text{ mJy}$ at $\alpha = 16^{\text{h}} 47^{\text{m}} 29^{\text{s}}.37$, $\delta = -29^{\circ} 19' 05''$).
245. *NGC 6215*.—Pair with NGC 6221.
246. *NGC 6221*.—Pair with NGC 6215.
248. *NGC 6300*.—Seyfert 2.
252. *IC 4662*.—Irr galaxy with bright H II regions and no visible radio nucleus.
253. *IRAS 17578–0400*.—In group of three galaxies, all of which may contribute to the *IRAS* source.
254. *IC 4687/6*.—IC 4689 ($S = 24.7 \text{ mJy}$ at $\alpha = 18^{\text{h}} 13^{\text{m}} 40^{\text{s}}.22$, $\delta = -57^{\circ} 44' 53''$) might contribute slightly to the *IRAS* source.
256. *IRAS F18293–3413*.—The $S_p = 13.5 \text{ mJy beam}^{-1}$ unresolved radio source at $\alpha = 18^{\text{h}} 32^{\text{m}} 44^{\text{s}}.86$, $\delta = -34^{\circ} 13' 44''$ appears to be an unrelated optically faint background galaxy.
258. *NGC 6744*.—This very extended (LAS $\approx 15'$) galaxy has a very faint ($S = 0.26 \text{ mJy}$) unresolved radio nucleus.
259. *NGC 6753*.—The $S = 148 \text{ mJy}$ flux density does not include the $S = 3.5 \text{ mJy}$ compact source at $\alpha = 19^{\text{h}} 11^{\text{m}} 20^{\text{s}}.0$, $\delta = -57^{\circ} 02' 37''$.
260. *ESO 593-IG008*.—Merging pair of galaxies.
265. *NGC 6822*.—Our 1.28 GHz flux density and position of this large, patchy, low-brightness irregular galaxy are very uncertain. See Cannon et al. (2006) for a detailed study of the FIR and radio emission from NGC 6822.
267. *ESO 339-G011*.—Radio-loud ($q = 1.73$) Seyfert 2 galaxy.
272. *IC 5063*.—Radio-loud ($q = 0.67$) warm [$\alpha(25 \mu\text{m}, 60 \mu\text{m}) = -0.46$] Seyfert 2 AGN core with radio plume. Serendipitous background ($V_h = 18052 \text{ km s}^{-1}$) giant radio galaxy at $\alpha = 20^{\text{h}} 51^{\text{m}} 39^{\text{s}}.8$, $\delta = -57^{\circ} 04' 34''$ (L. Marchetti et al. 2021, in prep).
276. *NGC 7083*.—No clearcut radio nucleus.
277. *NGC 7090*.—Asymmetric edge-on spiral disk, no clearcut radio nucleus.
278. *ESO 343-IG013*.—Interacting pair of galaxies.
281. *NGC 7205*.—No visible radio nucleus.
286. *ESO 239-IG002*.—Unresolved merging pair of galaxies.
290. *ESO 18-IG002*.—Unresolved merging pair of galaxies.
292. *NGC 7582*.—Seyfert 2. Background radio-loud BL Lac object MCG 07-47-031 at $\alpha = 23^{\text{h}} 19^{\text{m}} 05^{\text{s}}.93$, $\delta = -42^{\circ} 06' 48''$.

- 293. *NGC 7592*.—Interacting triple system.
- 294. *NGC 7590*.—Seyfert 2.
- 296. *ESO 077-IG014*.—Interacting pair of galaxies.
- 298. *NGC 7793*.—Faint extended emission with numerous H II regions superimposed, no clearcut radio nucleus.

4. SUMMARY

The MeerKAT Atlas comprises 1.28 GHz images of the 298 RBGS external galaxies with $|b| > 5^\circ$ in the southern hemisphere that are stronger than $S = 5.24 \text{ Jy}$ at $\lambda = 60 \mu\text{m}$. These images have $\theta \approx 7''.5$ FWHM resolution, or $\approx 1.8 \text{ kpc}$ at the median angular-size distance $\langle D_A \rangle \approx 50 \text{ Mpc}$ of RBGS galaxies. Each galaxy was observed with only $5 \times 3 \text{ min}$ snapshots, but the large number of MeerKAT antennas (64) gave good (u, v) -plane coverage and enabled accurate imaging of complex sources. The central portions of these images in FITS format can be downloaded from <https://doi.org/10.48479/dnt7-6q05>.

The typical rms image fluctuation $\sigma \approx 20 \mu\text{Jy beam}^{-1}$ is a combination of $\sigma_n \approx 15 \mu\text{Jy beam}^{-1}$ thermal noise, $\sigma_c \approx 2 \mu\text{Jy beam}^{-1}$ rms confusion from numerous faint sources, and residual sidelobes from strong sources in the $\Theta_{1/2} \approx 68'$ FWHM primary beam. The corresponding surface-brightness noise $\sigma \approx 0.26 \text{ K}$ at 1.28 GHz is low enough to reveal most disk emission from SFGs with about the same angular resolution as *Herschel* at $\lambda = 100 \mu\text{m}$ or *WISE* at mid-infrared wavelengths. Thus each MeerKAT image is sufficient to completely image a nearby galaxy in detail, and many images reveal low-brightness features not previously seen. In contrast, early VLA atlases (Condon et al. 1990, 1996) required two or more images per galaxy, a high-resolution image to isolate and resolve compact components and a low-resolution image to detect low-brightness extended emission.

The Atlas images are based on $5 \times 3 \text{ min}$ snapshots, so full tracks on individual sources would bring the rms image fluctuations much closer to the confusion limit $\sigma \gtrsim \sigma_c \approx 2 \mu\text{Jy beam}^{-1}$. *S*-band receivers covering 1.75 to 3 GHz currently being added to MeerKAT will lengthen the spectral baseline to allow more accurate measurements of continuum spectral indices and also bring higher angular resolution.

¹ The MeerKAT telescope is operated by the South African Radio Astronomy Observatory, which is a facility of the National Research Foundation, an agency of the Department of Science and Innovation. The National Radio Astronomy Observatory is a facility of the National Science Foundation operated by Associated Universities, Inc. This material is based upon work supported by the National Science Foundation Graduate Research Fellowship under Grant No. DDGE-1315231.
¹⁰ Support for this work was provided by the NSF through the Grote Reber Fellowship Program administered by Associated Universities, Inc./National Radio Astronomy Observatory. THJ acknowledges support from the National Research Foundation (South Africa). This research has made use of the NASA/IPAC Infrared Science Archive, which is funded by the National Aeronautics and Space Administration and operated by the California Institute of Technology. We thank the anonymous referee for a careful reading and detailed suggestions for clarifying our manuscript.

Facilities: Gaia, IRSA, MeerKAT, NED

REFERENCES

- Aalto, S., Falstad, N., Muller, S., et al. 2020, A&A, 640, A104, doi: [10.1051/0004-6361/202038282](https://doi.org/10.1051/0004-6361/202038282)
- Adebahr, B., Krause, M., Klein, U., et al. 2013, A&A, 555, A23, doi: [10.1051/0004-6361/201220226](https://doi.org/10.1051/0004-6361/201220226)
- Armus, L., Mazzarella, J. M., Evans, A. S., et al. 2009, PASP, 121, 559, doi: [10.1086/600092](https://doi.org/10.1086/600092)
- Cannon, J. M., & Skillman, E. D. 2004, ApJ, 610, 772, doi: [10.1086/421903](https://doi.org/10.1086/421903)
- Cannon, J. M., Walter, F., Armus, L., et al. 2006, ApJ, 652, 1170, doi: [10.1086/508341](https://doi.org/10.1086/508341)
- Charlot, P., Jacobs, C. S., Gordon, D., et al. 2020, A&A, 644, A159, doi: [10.1051/0004-6361/202038368](https://doi.org/10.1051/0004-6361/202038368)
- Chu, J. K., Sanders, D. B., Larson, K. L., et al. 2017, ApJS, 229, 25, doi: [10.3847/1538-4365/aa5d15](https://doi.org/10.3847/1538-4365/aa5d15)
- Cluver, M. E., Jarrett, T. H., Dale, D. A., et al. 2017, ApJ, 850, 68, doi: [10.3847/1538-4357/aa92c7](https://doi.org/10.3847/1538-4357/aa92c7)
- Condon, J. J. 1992, ARA&A, 30, 575, doi: [10.1146/annurev.aa.30.090192.003043](https://doi.org/10.1146/annurev.aa.30.090192.003043)
- Condon, J. J., Cotton, W. D., Greisen, E. W., et al. 1998, AJ, 115, 1693, doi: [10.1086/300337](https://doi.org/10.1086/300337)
- Condon, J. J., Helou, G., Sanders, D. B., & Soifer, B. T. 1990, ApJS, 73, 359, doi: [10.1086/191472](https://doi.org/10.1086/191472)
- . 1996, ApJS, 103, 81, doi: [10.1086/192270](https://doi.org/10.1086/192270)
- Condon, J. J., Matthews, A. M., & Broderick, J. J. 2019, ApJ, 872, 148, doi: [10.3847/1538-4357/ab0301](https://doi.org/10.3847/1538-4357/ab0301)
- Cotton, W. D. 2008, PASP, 120, 439, doi: [10.1086/586754](https://doi.org/10.1086/586754)
- Cotton, W. D., Condon, J. J., Kellermann, K. I., et al. 2018, ApJ, 856, 67, doi: [10.3847/1538-4357/aaaec4](https://doi.org/10.3847/1538-4357/aaaec4)
- Cotton, W. D., Thorat, K., Condon, J. J., et al. 2020, MNRAS, 495, 1271, doi: [10.1093/mnras/staa1240](https://doi.org/10.1093/mnras/staa1240)
- de Grijs, M. H. K., Miley, G. K., Lub, J., & de Jong, T. 1985, Nature, 314, 240, doi: [10.1038/314240a0](https://doi.org/10.1038/314240a0)
- Elagali, A., Wong, O. I., Oh, S.-H., et al. 2018, MNRAS, 476, 5681, doi: [10.1093/mnras/sty741](https://doi.org/10.1093/mnras/sty741)
- Fernández, X., van Gorkom, J. H., Schweizer, F., & Barnes, J. E. 2010, AJ, 140, 1965, doi: [10.1088/0004-6256/140/6/1965](https://doi.org/10.1088/0004-6256/140/6/1965)
- Harnett, J., Ehle, M., Fletcher, A., et al. 2004, A&A, 421, 571, doi: [10.1051/0004-6361:20034377](https://doi.org/10.1051/0004-6361:20034377)
- Helou, G., Soifer, B. T., & Rowan-Robinson, M. 1985, ApJL, 298, L7, doi: [10.1086/184556](https://doi.org/10.1086/184556)
- Hummel, E. 1981, A&A, 93, 93
- Hummel, E., van der Hulst, J. M., & Keel, W. C. 1987, A&A, 172, 32
- Laing, R. A., Riley, J. M., & Longair, M. S. 1983, MNRAS, 204, 151, doi: [10.1093/mnras/204.1.151](https://doi.org/10.1093/mnras/204.1.151)
- Mauch, T., Jarrett, T., Cotton, W. D., & Condon, J. J. 2020a, Snapshot Observations with MeerKAT. <https://archive-gw-1.kat.ac.za/public/meerkat/Snapshot-Observations-with-MeerKAT.pdf>
- Mauch, T., Murphy, T., Buttery, H. J., et al. 2003, MNRAS, 342, 1117, doi: [10.1046/j.1365-8711.2003.06605.x](https://doi.org/10.1046/j.1365-8711.2003.06605.x)
- Mauch, T., Cotton, W. D., Condon, J. J., et al. 2020b, ApJ, 888, 61, doi: [10.3847/1538-4357/ab5d2d](https://doi.org/10.3847/1538-4357/ab5d2d)
- Murphy, E. J., Helou, G., Kenney, J. D. P., Armus, L., & Braun, R. 2008, ApJ, 678, 828, doi: [10.1086/587123](https://doi.org/10.1086/587123)
- Neugebauer, G., Habing, H. J., van Duinen, R., et al. 1984, ApJL, 278, L1, doi: [10.1086/184209](https://doi.org/10.1086/184209)
- Reynolds, J. E. 1994, ATNF Memo, AT/39.3/040
- Rice, W., Lonsdale, C. J., Soifer, B. T., et al. 1988, ApJS, 68, 91, doi: [10.1086/191283](https://doi.org/10.1086/191283)
- Sanders, D. B., Mazzarella, J. M., Kim, D. C., Surace, J. A., & Soifer, B. T. 2003, AJ, 126, 1607, doi: [10.1086/376841](https://doi.org/10.1086/376841)
- Sanders, D. B., & Mirabel, I. F. 1996, ARA&A, 34, 749, doi: [10.1146/annurev.astro.34.1.749](https://doi.org/10.1146/annurev.astro.34.1.749)
- Schmitt, H. R., Calzetti, D., Armus, L., et al. 2006, ApJS, 164, 52, doi: [10.1086/501529](https://doi.org/10.1086/501529)
- Skrutskie, M. F., Cutri, R. M., Stiening, R., et al. 2006, AJ, 131, 1163, doi: [10.1086/498708](https://doi.org/10.1086/498708)